

An-Najah National University
Faculty of Graduate studies

**Structural, electronic, magnetic and elastic properties
in the Full-Heusler Compounds: Co_2CrAl , Cr_2MnSb
using FP-LAPW Method**

By
Sara Jamal Mohammad Yahya

Supervisor
Prof. Mohammed Abu-Jafar

**This Thesis is Submitted in Partial Fulfillment of the Requirements for
the Degree of Master of physics, Faculty of Graduate Studies, An-
Najah National University, Nablus, Palestine.**

2021

**Structural, electronic, magnetic and elastic properties
in the Full-Heusler Compounds: Co_2CrAl , Cr_2MnSb
using FP-LAPW Method**

By

Sara Jamal Mohammad Yahya

This Thesis was Defended Successfully on 28 /4/2021 and Approved by:

Defense Committee Members:

Signature

- Prof. Mohammed Abu-Jafar / Supervisor

Moh'd.....

- Dr. Raed Jaradat / External Examiner

Raed Jaradat.....

- Dr. Mahmoud Farout / Internal Examiner

.....*M. Farout*.....

Dedication

I am highly grateful to my beloved parents for all the sacrifices they have made to make my future better. ALLAH bless them. To my beloved fiancé (Saleh), who shares me all moments and helps me to overcome difficulties to continue moving forward. To my lovely brothers (Mohammad, Abd-Allah, Ibrahim and Yamen), who always encourage me and give me a powerful support.

Acknowledgments

All thanks to Allah, who gives me health, knowledge and patience to complete my thesis. I would like to acknowledge the following people who helped me in many aspects that made me possible to write this thesis. At first, I address a special thanks to my supervisor and instructor Prof. Dr. Mohammed Abu-Jafar for his continuous supports, effortless helps, valuable discussions and humble guidance. He always encourages my work and allows me to think and execute my plans independently. I really feel so lucky to have him as my supervisor. Never forget my faculty members of physics department for their help and encouragement.

الاقرار

انا الموقعة ادناه مقدمة الرسالة التي تحمل العنوان:

Structural, electronic, magnetic and elastic properties in the Full-Heusler Compounds: Co_2CrAl , Cr_2MnSb using FP-LAPW Method

أقر بأن ما اشتملت عليه هذه الرسالة إنما هي نتاج جهدي الخاص، باستثناء ما تمت الإشارة اليه حيثما ورد، وأن هذه الرسالة ككل، أو أي جزء منها لم يقدم من قبل لنيل أية درجة علمية أو بحث علمي لدى أية مؤسسة تعليمية أو بحثية أخرى.

Declaration

The work provided in this thesis, unless otherwise referenced, is the researcher's own work, and has not been submitted elsewhere for any other degree or qualification.

Student's Name: Sara Jamal Mohammad Yahya اسم الطالبة:

Signature:  التوقيع:

Date: 28 / 4 / 2021 التاريخ:

Table of contents

No.	content	Page
	Dedication	iii
	Acknowledgment	iv
	الإقرار	v
	Table of contents	vi
	List of Tables	vii
	List of Figures	viii
	Abstract	xi
1	Chapter One: Introduction	1
2	Chapter two: Methodology	5
2.1	The Open-Heimer Approximation	5
2.2	Hartree and Hartree-Fock Approximation	6
2.3	Density Functional Theory	6
2.4	Single Particle Kohn-Sham Equation	7
2.5	The Exchange-Correlation Functional	9
2.6	Local Density Approximation (LDA)	10
2.7	Generalized Gradient Approximation (GGA)	11
2.8	modified Becke-Johnson potential	11
2.9	Augmented Plane Wave (APW) Method	12
2.10	The Linearized Augmented Plane Wave (LAPW) Method	13
3	Chapter Three: Results and Discussion	15
3.1	Computational Method	15
3.2	Structural Properties	16
3.3	Magnetic Properties	22
3.4	Electronic Properties	25
3.5	Elastic properties	42
4	Chapter Four: Conclusion	46
	References	48
	الملخص	ب

List of Tables

No.	Table captions	Page
1	Calculated lattice parameter (a), bulk modulus (B), pressure derivative (B'), c/a and total energy for Heusler Co_2CrAl compound.	19
2	Calculated lattice parameter (a), bulk modulus (B), pressure derivative (B'), c/a and total energy for Heusler Cr_2MnSb compound.	20
3	Total magnetic moment for inverse, normal and tetragonal I4/mmm (139) Heusler Co_2CrAl compounds.	23
4	Total magnetic moment for inverse, normal and tetragonal I4/mmm (139) Heusler Cr_2MnSb compounds.	24
5	Energy band gaps for normal and inverse Co_2CrAl compound using PBE-GGA and mBJ methods.	32
6	Energy band gaps for normal and inverse Cr_2MnSb compound using PBE-GGA and mBJ methods.	32
7	Energy band gaps for Tetragonal I4/mmm (139) Heusler (Co_2CrAl , Cr_2MnSb) compounds in AFM state.	32
8	Voigt bulk modulus (B), Voigt shear modulus (S), elastic constants (C_B), B/S ratio, Voigt Poisson's ratio (ν), Voigt Young's modulus (Y) and anisotropic factor (A) of the FM normal and inverse Heusler (Co_2CrAl , Cr_2MnSb) compounds.	45

List of Figures

No.	Figure captions	Page
1	Flow chart for the n^{th} iteration in the self-consistent procedure to solve Hartree-Fock or Kohn-Sham equations.	9
2	Partitioning of the unit cell into atomic spheres (I) and an interstitial region (II).	13
3	Different crystal structures of Heusler Co_2CrAl a) normal Heusler structure Co_2CrAl Fm-3m (225), b) inverse Heusler Co_2CrAl structure F-43m (216), c) Tetragonal structure I4/mmm (139), d) Tetragonal structure I-4m2 (119).	17
4	The total energy (Ry) versus volume (a.u. ³) for different crystal structure of Co_2CrAl Heusler.	18
5	The total energy (Ry) versus volume (a.u. ³) for different crystal structures of Cr_2MnSb Heusler.	18
6	The band structure for inverse Heusler Co_2CrAl compound by using PBE-GGA method for (a) spin up inverse Heusler Co_2CrAl compound (b) spin down inverse Heusler Co_2CrAl compound.	27
7	The band structure for inverse Heusler Co_2CrAl compound by using mBJ-GGA method for (a) spin up inverse Heusler Co_2CrAl compound (b) spin down inverse Heusler Co_2CrAl compound.	27
8	The band structure for normal Heusler Co_2CrAl compound by using PBE-GGA method for (a) spin up normal Heusler Co_2CrAl compound (b) spin down normal Heusler Co_2CrAl compound.	28
9	The band structure for normal Heusler Co_2CrAl compound by using mBJ-GGA method for (a) spin up normal Heusler Co_2CrAl compound (b) spin down normal Heusler Co_2CrAl compound.	28
10	The band structure for inverse Heusler Cr_2MnSb compound by using PBE-GGA method for (a) spin up inverse Heusler Cr_2MnSb compound (b) spin down inverse Heusler Cr_2MnSb compound.	29
11	The band structure for inverse Heusler Cr_2MnSb compound by using mBJ-GGA method for (a) spin up inverse Heusler Cr_2MnSb compound (b) spin down	29

	inverse Heusler Cr_2MnSb compound.	
12	The band structure for normal Heusler Cr_2MnSb compound by using PBE-GGA method for (a) spin up normal Heusler Cr_2MnSb compound (b) spin down normal Heusler Cr_2MnSb compound.	30
13	The band structure for normal Heusler Cr_2MnSb compound by using mBJ-GGA method for (a) spin up normal Heusler Cr_2MnSb compound (b) spin down normal Heusler Cr_2MnSb compound.	30
14	The band structure for Tetragonal I4/mmm (139) Heusler Co_2CrAl compound in AFM state (a) spin up Tetragonal I4/mmm Heusler (139) Co_2CrAl compound (b) spin down Tetragonal I4/mmm Heusler (139) Co_2CrAl compound.	31
15	The band structure for Tetragonal I4/mmm (139) Heusler Cr_2MnSb compound in AFM state (a) spin up Tetragonal I4/mmm Heusler (139) Cr_2MnSb compound (b) spin down Tetragonal I4/mmm Heusler (139) Cr_2MnSb compound.	31
16	(a) Total density of states of spin up for inverse Co_2CrAl and partial density of states of spin up for (b) Co atom (c) Cr atom (d) Al atom of inverse Co_2CrAl compound.	34
17	(a) Total density of states of spin down for inverse Co_2CrAl and partial density of states of spin up for (b) Co atom (c) Cr atom (d) Al atom of inverse Co_2CrAl compound.	35
18	(a) Total density of states of spin up for normal Co_2CrAl and partial density of states of spin up for (b) Co atom (c) Cr atom (d) Al atom of normal Co_2CrAl compound.	36
19	(a) Total density of states of spin down for normal Co_2CrAl and partial density of states of spin up for (b) Co atom (c) Cr atom (d) Al atom of normal Co_2CrAl compound.	37
20	(a) Total density of states of spin up for inverse Cr_2MnSb and partial density of states of spin up for (b) Cr atom (c) Mn atom (d) Sb atom of inverse Cr_2MnSb compound.	38
21	(a) Total density of states of spin down for inverse Cr_2MnSb and partial density of states of spin up for (b) Cr atom (c) Mn atom (d) Sb atom of inverse	39

	<i>Cr₂MnSb</i> compound.	
22	(a) Total density of states of spin up for normal <i>Cr₂MnSb</i> and partial density of states of spin up for (b) Cr atom (c) Mn atom (d) Sb atom of normal <i>Cr₂MnSb</i> compound.	40
23	(a) Total density of states of spin down for normal <i>Cr₂MnSb</i> and partial density of states of spin up for (b) Cr atom (c) Mn atom (d) Sb atom of normal <i>Cr₂MnSb</i> compound.	41

Structural, electronic, magnetic and elastic properties in the Full-Heusler Compounds: Co_2CrAl , Cr_2MnSb using FP-LAPW Method

By

Sara Jamal Mohammad Yahya**Supervisor****Prof. Mohammed Abu-Jafar****Abstract**

Structural, electronic, magnetic and elastic properties of the Full-Heusler Compounds Co_2CrAl , Cr_2MnSb have been investigated using full potential linearized augmented plane wave (FP-LAPW) method. The FP-LAPW method is a procedure for solving the Kohn-Sham equations for the total energy of a many-electron system by calculating the structural parameters (lattice parameters, c/a , total energy bulk modulus, and first pressure derivatives of bulk modulus). The Generalized Gradient Approximation (GGA) has been used for the exchange-correlation potential (V_{xc}) to find the structural parameters. The energy band gaps for these compounds have been investigated by the modified Becki-Johnson potential (mBJ). The normal Heusler Co_2CrAl compound within GGA and mBJ approaches are found to have a half-metallic behavior, with indirect energy gap in the spin down configuration, while the normal, inverse Heusler Cr_2MnSb and tetragonal (139) (Co_2CrAl , Cr_2MnSb) compounds are found to have a half-metallic behavior, with direct energy gap. The total magnetic moments for these compounds are to some extent compatible with experimental and theoretical results. Therefore, the normal and inverse Full-Heusler compound Co_2CrAl is mechanically stable. But, the inverse Cr_2MnSb is mechanically instable in ferromagnetic state. On the other hand the normal Cr_2MnSb is mechanically stable in ferromagnetic state.

Chapter One

Introduction

Since their discovery in 1903, Heusler compounds have many applications includes Spintronic^[1], Shape memory^[2] and thermoelectric^[3]. Heusler compounds are a type of face-centered cubic crystal structure (fcc). They can be divided in two groups: XYZ (Half-Heuslers) which consisting of three fcc sub-lattices and X_2YZ (Full-Heuslers) which have four fcc sub-lattices. where X and Y are transition elements and Z is s,p,... elements^[4].

The Full-Heusler X_2YZ compounds crystallize in two types normal and inverse. the normal Heusler crystallizes in Cu_2MnAl structure with space group of $Fm\bar{3}m$ (space group number 225)^[5] and atomic positions of X_2 : $(1/4,1/4,1/4)$, $(3/4,3/4,3/4)$, $Y(1/2,1/2,1/2)$ and $Z(0,0,0)$ ^[5]. Therefore, the inverse Heusler crystallizes in Hg_2CuTi with space group of $F\bar{4}3m$ (space group number 216)^[5]and atomic positions of X_2 : $(1/4,1/4,1/4)$, $(1/2,1/2,1/2)$, $Y(3/4,3/4,3/4)$ and $Z(0,0,0)$.

Heusler compounds have half-metallic (HM) character. Therefore, half-metals have only one spin channel for conduction: the spin-polarized band structure exhibits metallic behavior for one spin channel, while the other spin band structure exhibits a gap at the Fermi level, so half-metallic materials exhibiting a 100% spin polarization ^[6-18].

There are some studies about Heusler alloys properties like structural, elastic, magnetic and electronic properties by using different methods. In 2004 Zhang *et al.* ^[19] studied the electronic band structure and transport

properties for Co_2CrAl Heusler compound. They measured the lattice parameter, magnetic moment and indirect band gap for Co_2CrAl Heusler compound and found to be 5.73 \AA , $3\mu_B$, 0.475 eV . In 2010 Hakimi *et al.* ^[20] studied the structural and magnetic properties of Co_2CrAl compound prepared by mechanical alloying. They found the total magnetic moment for normal Co_2CrAl to be $2\mu_B$.

In 2009 Ozdogan and Galanakis ^[21] determined the electronic and magnetic properties of the half-metallic antiferromagnetic Cr_2MnSb . They studied the electronic and magnetic properties of the Cr_2MnSb full-Heusler alloy using ab-initio electronic structure calculations for both normal and inverse types. They found that for both structural types Cr_2MnSb is a half-metallic ferrimagnet compound for a wide range of lattice constants.

Heusler alloys are well-known for their potential application in spin-transfer torque in spin-transfer torque (STT). These materials crystallize in multifaceted structure in both cubic and tetragonal with multiple magnetic sub-lattices. Gupta *et al.* ^[22] recently deposit Cr_2MnSb thin films on a MgO (001) substrate in crystalized phase shows cubic structure with full B2 and partial L21 ordering.

In 2017, Atsufumi Hirohata ^[23] *et al.* focused on AFM Heusler alloys and established correlations between their crystalline structures and magnetic properties, i.e. antiferromagnetism. Heusler alloys consisting of elements with moderate magnetic moments require perfectly or partially ordered crystalline structures to exhibit AFM behavior. By using elements with

large magnetic moments, even a fully disordered structure is found to show either AFM or ferromagnetic (FI) behavior. The latter alloys may become useful for device applications by additional increase of their anisotropy and grain volume to maintain the AFM behavior above room temperature. Recent research on new antiferromagnetic Heusler alloys and their exchange interactions along the plane normal is discussed. These new antiferromagnets are characterized by very sensitive magnetic and electrical measurement techniques recently developed to determine their characteristic temperatures together with atomic structural analysis.

Recently, Abu Baker *et al.* ^[24] investigated the structural, magnetic, electronic and elastic properties of half-metallic ferro-magnetism full-Heusler alloys: Normal- Co_2TiSn and inverse- Zr_2RhGa using FP-LAPW method. The lattice parameter for Normal- Co_2TiSn and inverse- Zr_2RhGa are found to be respectively 6.094 \AA and 6.619 \AA . Also the total magnetic moment for these compounds found to be $1.9786 \mu_B$ and $1.99 \mu_B$ respectively. The normal Co_2TiSn and inverse Zr_2RhGa compounds have an indirect energy gap of 0.482 eV and 0.573 eV , respectively. The elastic properties indicate that the normal full Heusler Co_2TiSn compound and the inverse full Heusler Zr_2RhGa compounds are mechanically stable.

The motivation of this study is to investigate the structural, electronic, magnetic and elastic properties of the Full-Heusler Compounds Co_2CrAl , Cr_2MnSb by using full potential linearized augmented plane wave (FP-LAPW) method. The methodology is presented in chapter two. In chapter

three we will show our results and discussion. Finally, Conclusion is summarized in chapter four.

Chapter Two Methodology

Unfortunately the Schrodinger equation for an N-body system; given in equation 1 below; is very hard to be solved. Obviously we have to have certain approximations to deal with the various body problems ^[25, 26]. The Hamiltonian operator (\hat{H}) is given by:

$$\hat{H} = -\frac{\hbar^2}{2} \sum_{i=1}^N \frac{\nabla_{\vec{R}_i}^2}{M_i} - \frac{\hbar^2}{2} \sum_{i=1}^N \frac{\nabla_{\vec{r}_i}^2}{m_e} - \frac{1}{4\pi\epsilon_0} \sum_{ij}^N \frac{e^2 Z_i}{|\vec{R}_i - \vec{r}_j|} + \frac{1}{8\pi\epsilon_0} \sum_{i \neq j}^N \frac{e^2}{|\vec{r}_i - \vec{r}_j|} + \frac{1}{8\pi\epsilon_0} \sum_{i \neq j}^N \frac{e^2 Z_i Z_j}{|\vec{R}_i - \vec{R}_j|} \quad (1)$$

The first term is the kinetic energy operator for the nuclei (T_n), the second for the electrons (T_e). The last three term describe the coulomb interaction between electron and others electrons (V_{ee}), between electron and nuclei (V_{en}) and between nuclei and other nuclei (V_{nn}). This Schrodinger equation for many body problem system doesn't have an exact solution. There are some approximations to solve this problem:

2.1 The Open-Heimer Approximation:

This approximation^[25] proposed that the nuclei are more massive than electrons, therefore, the kinetic energy operator for the electrons is equal to zero and the coulomb interaction between a nucleus and other nuclei is constant and then the Hamiltonian is written as:

$$H = T_e + V_{ee} + V_{ext} \quad (2)$$

where the external potential is given by $V_{ext} = V_{nn} + V_{en}$

2.2 Hartree and Hartree-Fock Approximation:

Hartree approximation^[25] is based on Pauli Exclusion Principle: no two electrons are permitted to have the same set of quantum numbers. The other particle system solved in Hartree-Fock approximation by assuming that the electrons are independent of each other. Electrons' wave function can be written as:

$$\Psi(r_1, r_2, r_3, \dots, r_N) = \Psi_1(r_1) \Psi_2(r_2) \Psi_3(r_3) \dots \Psi_N(r_N) \quad (3)$$

where $\Psi_N(r_N)$ is the wave function for the electron (N). The total Hamiltonian can be written as:

$$H = (T_s + V_{ext} + V_H)(r) \quad (4)$$

where T_s is the kinetic energy, V_{ext} is the external potential and V_H is the Hartree potential for non-interacting electrons.

$$V_H \text{ can be written as : } V_H = \frac{1}{8\pi\epsilon_0} \sum_{ij}^N \frac{|\psi(r_i)|^2 |\psi(r_j)|^2 d^3r_i d^3r_j}{|\vec{r}_i - \vec{r}_j|} \quad (5)$$

2.3 Density Functional Theory:

Density functional^[25] theory allows the proper treatment of the Coulomb correlation as it introduces an exchange correlation term within the one-electron approximation. It takes into account the exchange correlation in interacting systems and only kinetic energy in non-interacting systems. It relies on the approximation of the unknown exchange correlation functional of the charge density. It is applicable in systems where the electron distribution is no longer homogenous. DFT manages many body problems on a single body problem. Its efficient minimization of the functional energy would lead to the density of the ground state (ρ_0). Thus

$E(\rho)$ is rewritten as the Hartree total energy plus another smaller unknown functional called exchanged-correlation functional, $E_{xc}(\rho)$.

$$\mathbf{E}(\boldsymbol{\rho}) = \mathbf{T}_s(\boldsymbol{\rho}) + \mathbf{E}_c(\boldsymbol{\rho}) + \mathbf{E}_H(\boldsymbol{\rho}) + \mathbf{E}_{ii}(\boldsymbol{\rho}) + \mathbf{E}_{xc}(\boldsymbol{\rho}) \quad (6)$$

where T_s is single electron kinetic energy, E_c is the Coloumb energy between nuclei and electrons, $E_{ii}(\rho)$ is the interaction between nuclei, E_{xc} is the exchange correlation energy is unknown part and, E_H is the Hartree potential energy, which is defined as follow.

$$\mathbf{E}_H(\boldsymbol{\rho}) = \frac{e^2}{2} \int \mathbf{d}^3 \mathbf{r} \mathbf{d}^3 \mathbf{r}' \frac{\rho(\vec{r})\rho(\vec{r}')}{|\vec{r}-\vec{r}'|} \quad (7)$$

Therefore, Schrodinger equation of a one electron can be written asfollow:

$$[\mathbf{T}_s + \mathbf{V}_{ext}(\mathbf{r}) + \mathbf{V}_H(\boldsymbol{\rho}(\mathbf{r})) + \mathbf{V}_{XC}(\boldsymbol{\rho}(\mathbf{r}))]\Phi_i(\mathbf{r}) = \varepsilon_i \Phi_i(\mathbf{r}) \quad (8)$$

where, ε_i is the single particle energy, φ_i is the electron wave function, V_H is the Hartree potential, V_{ext} is the coulomb potential and V_{XC} is the exchange-correlation potential.

2.4 Single Particle Kohn-Sham Equation:

The LAPW method is a technique for solving the Kohn-Sham equations^[25] of a many-electron system. We should view the above term as the functional energy of a non-interacting classical electron gas, subjected to two external potentials: one attributable to the nuclei $\widehat{V}_{ext}[\rho]$, and the other attributable to the exchange and correlation effects $\widehat{V}_{xc}[\rho]$. The exact ground-state density $\rho(\mathbf{r})$ of an N-electron system is:

$$\boldsymbol{\rho}(\vec{\mathbf{r}}) = \sum_{i=1}^N \boldsymbol{\Phi}_i^*(\vec{\mathbf{r}})\boldsymbol{\Phi}_i(\vec{\mathbf{r}}) = \sum_{i=1}^N |\boldsymbol{\Phi}_i(\vec{\mathbf{r}})|^2 \quad (9)$$

where the single-particle wave functions $\phi_i(\vec{\mathbf{r}})$ are the N lowest-energy solutions of the Kohn- Sham equation. This equation is defined as:

$$\hat{H}_{KS}\phi_i = \epsilon_i\phi_i \quad (10)$$

$$\hat{H}\phi_i(\vec{r}) = \left[-\frac{\hbar^2}{2m_e}\vec{\nabla}_i^2 + V_{\text{eff}} \right] \phi_i = \epsilon_i\phi_i \quad (11)$$

Equation (11) is another formula for Kohn-Sham equation. Where \hat{H} is known as the Hamiltonian operator. The effective potential $V_{\text{eff}}(\vec{r})$ is the sum of the external, the Hartree (electrostatic), and the exchange-correlation potentials:

$$\begin{aligned} V_{\text{eff}}(\vec{r}) = V_{\text{ext}}(\vec{r}) + \frac{\delta E_H[\rho]}{\delta \rho} + \frac{\delta E_{xc}[\rho]}{\delta \rho} &= V_{\text{ext}}(\vec{r}) + \frac{e^2}{4\pi\epsilon_0} \int \frac{\rho(\vec{r}')}{|\vec{r}-\vec{r}'|} d\vec{r}' + \\ V_{xc}(\vec{r}) & \end{aligned} \quad (12)$$

From equation (12), V_H and V_{xc} depends on the charge density $\rho(\vec{r})$, which in turn depends on ϕ_i which are being searched. That implies we are dealing with the question of self-consistency. The solution ϕ_i determine the original equation (V_H and V_{xc} in H_{KS}), and the equation cannot be written down and solved before its solution is known. Some starting density ρ_0 is guessed, and a Hamiltonian H_{KS1} can be constructed with it. The eigenvalue problem is solved, and ϕ_1 can be determined from ρ_1 . Now ρ_1 can be used to construct H_{KS2} which will yield ρ_2 , etc. The procedure can be used until the series converge and final density ρ_f get out. The flow chart for the n^{th} iteration in the self-consistent procedure to solve Hartree-Fock or Kohn-Sham equations is shown in Figure (1).

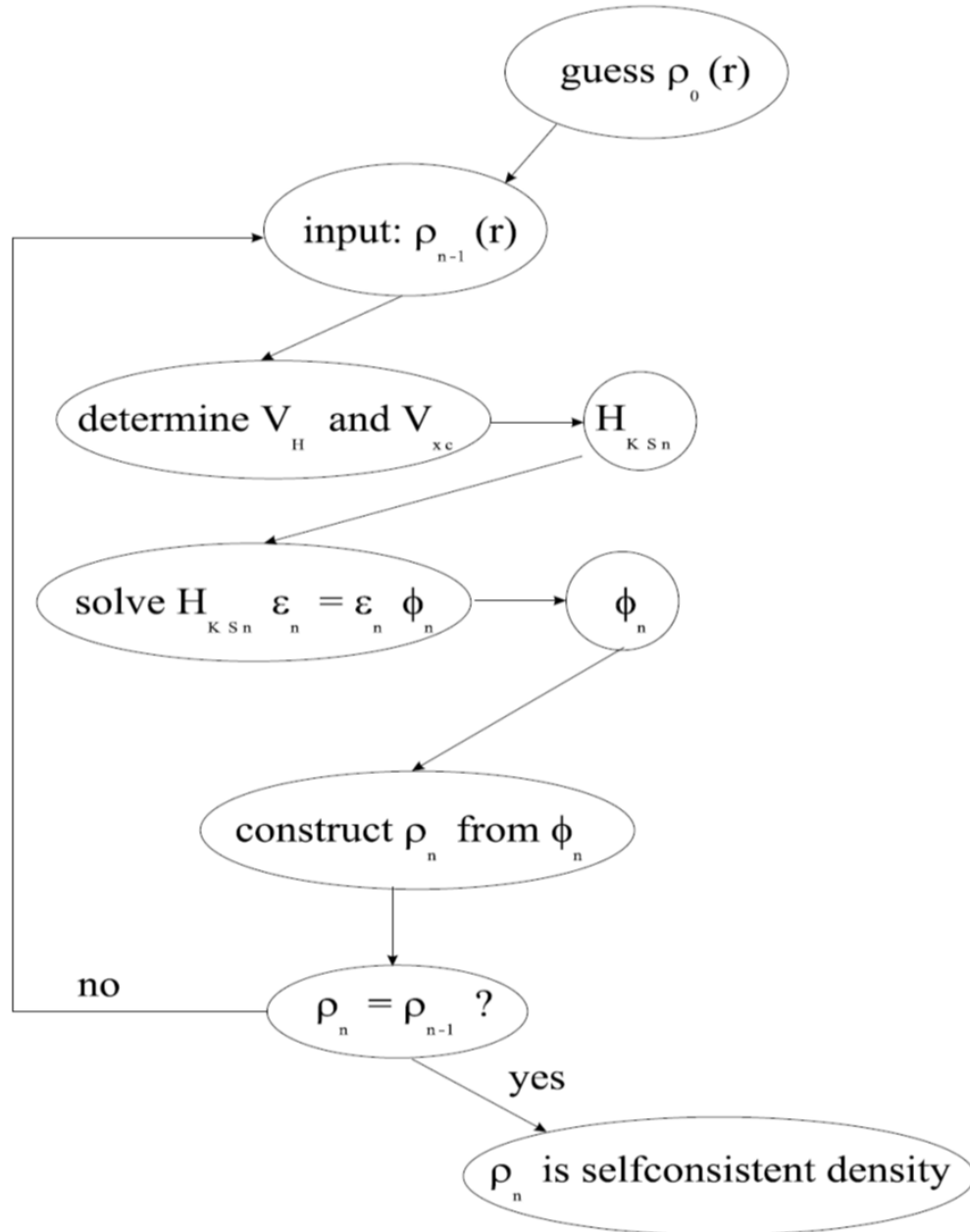


Figure (1): Flow chart for the n^{th} iteration in the self-consistent procedure to solve Hartree-Fock or Kohn-Sham equations.

2.5 The Exchange-Correlation Functional

The Kohn-Sham scheme mentioned above was accurate: no other approximations were made apart from the preceding Born-Oppenheimer approximation. But we have so far ignored the fact that we do not know the functional exchange-correlation. The introduction of an approximation is

needed. Two such often-used approximations are LDA (Local Density Approximation) and GGA (Generalized Gradient Approximation).

2.6 Local Density Approximation (LDA)

This approximation^[25] represents the simplest approach to $\varepsilon_{xc}[\rho(\vec{r})]$ which, in the context of this model, would be given by:

$$E_{xc}^{LDA} = \int \rho(\vec{r}) \varepsilon_{xc}[\rho(\vec{r})] d\vec{r} \quad (13)$$

where $\varepsilon_{xc}[\rho(\vec{r})]$ is the exchange-correlation energy per electron of a homogenous electron gas (a system formed by uniformly distributed electrons moving on a positive charge background so that the system is electrically neutral) whose electronic density is precisely $\rho_0(r)$ at each point r . The term “local” refers to the absence of any $\rho_0(r)$ derivative in the expression for $\varepsilon_{xc}[\rho(\vec{r})]$ given by equation (13) which implies that the LDA approximation will be valid when the electronic density varies very slowly with the position. If the exchange and correlation contributions are considered separately, the first one can be computed analytically. The correlation energy, in turn, lacks an analytical expression and is represented as a complicated function of ρ_0 depending on parameters whose values are fitted using accurate simulations for the energy of the homogeneous electron gas.

$$E_{xc}^{LDA} = E_x^{LDA} + E_c^{LDA} \quad (14)$$

The first term is the exchange energy that comes from the Pauli Exclusion Principle. The second term called the correlation energy E_c^{LDA} originates from the interaction of electrons having the same spin.

2.7 Generalized Gradient Approximation (GGA).

This approximation improves the LDA definition^[25] of the exchange-correlation energy by including the first derivatives of the electronic density. Whereas LDA uses the exchange energy density of the uniform electron gas, regardless of the homogeneity of the real charge density, the generalized gradient approximation takes care of such inhomogeneity (non-uniform charge density) by including the gradient of the electron density in the functional. GGA uses both charge density $\rho(\vec{r})$ and the gradient of the charge density $\vec{\nabla}\rho(\vec{r})$ to solve the exchange-correlation energy as shown in equation (15).

$$E_{xc}^{GGA} = \int \rho(\vec{r}) \varepsilon_{xc}[\rho(\vec{r}), \vec{\nabla}\rho(\vec{r})] d\vec{r} \quad (15)$$

2.8 Modified Becke-Johnson (mBJ) potential

mBJ potential is used in WIEN2k code^[27]. mBJ is an efficient tool used to improve the band structure of the materials especially for semiconductors and found to be an important in the overall agreement with experiment as Tran and Blaha^[26] did before for a more reduced set of semiconductors. We found within this enhanced set, that the deviation from the experimental gap value can reach even much more than 20%, in some cases. Furthermore, since there is no exchange and correlation energy term from which the mBJ-GGA potential can be deduced, a direct optimization procedure to get the lattice parameter in a consistent way is not possible as in the usual theory. These authors suggest that an LDA or GGA optimization procedure is used previously to a band structure calculation and the resulting lattice parameter introduced into the 2011 code. This

choice is important since small percentage differences in the lattice parameter can give rise to quite higher percentage deviations from experiment in the predicted band gap value.

2.9 Augmented Plane Wave (APW) Method.

This method is a procedure for solving the Kohn-Sham equations^[25]. In the region far away from the nuclei, the electrons are more or less ‘free’. Free electrons are described by plane waves. Close to the nuclei, the electrons behave quite as they were in a free atom, and they could be described more efficiently by atomic like functions. In the APW scheme the unit cell is partitioned into two types of regions as shown in Figure 2. i) non-overlapping spheres centered at the atomic sites such a sphere is often called a muffin tin sphere. ii) An interstitial region; the remaining space outside the spheres. One augmented plane wave (APW) used in the expansion of φ_n is defined as:

$$\phi_{\vec{k}}^{\vec{k}}(\vec{r}, E) = \begin{cases} \frac{1}{\sqrt{V}} e^{i(\vec{k}+\vec{K})\cdot\vec{r}} & , \quad \text{Outside sphere} \\ \sum_{l,m} A_{lm}^{\alpha, \vec{k}+\vec{K}} u_l^\alpha(r', E) Y_m^l(\hat{r}') & , \quad \text{Inside sphere} \end{cases} \quad (16)$$

where \vec{K} is the reciprocal lattice vectors and \vec{k} is the wave vector inside the Brillion zone, V is the volume of the unit cell, the position vector r' inside the sphere, u_l^α is the numerical solution to the radial Schrodinger equation at the energy ε .

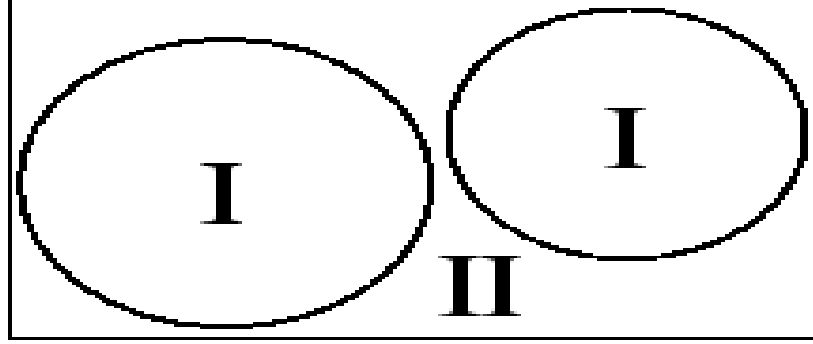


Figure (2): Partitioning of the unit cell into atomic spheres (I) and an interstitial region (II).

2.10 The Linearized Augmented Plane Wave (LAPW) Method.

This method^[25] is a procedure for solving the Kohn-Sham equations for the ground state density, total energy, and Kohn-Sham eigenvalues of a many-electron system by introducing a basis set which is especially adapted to the problem. (LAPW) scheme proposed by Andersen (who suggested expanding the energy dependency of radial wave functions $u(r')$ inside the atomic spheres with its energy derivative $\frac{\partial u^\alpha(r', E)}{\partial E} = \dot{u}^\alpha(r', E)$, a linear combination of radial function times spherical harmonics is used in this scheme. Spherical harmonic $Y_{lm}(r)$ is used where $u_l(r, E_l)$ is the regular solution of the radial Schrödinger equation for energy E_l and the spherical part of the potential inside sphere $\dot{u}^\alpha(r', E)$ is the energy derivative of u_l taken at the same energy E_l .

$$\Phi_{\vec{K}}^{\vec{k}}(\vec{r}, \mathbf{E}) = \sum_{l,m} (\mathbf{a}_{lm}^{\alpha, \vec{k}+\vec{K}} u_l^\alpha(r', \mathbf{E}) + \mathbf{b}_{lm}^{\alpha, \vec{k}+\vec{K}} \dot{u}_l^\alpha(r', \mathbf{E})) Y_m^l(\hat{r}'), \text{ Inside sphere } \quad (17)$$

In the interstitial region, a plane wave function from equation (18).

$$\begin{aligned} & \phi_{\vec{K}}^{\vec{k}}(\vec{r}, E) \\ &= \frac{1}{\sqrt{V}} e^{i(\vec{k}+\vec{K})\cdot\vec{r}} \quad , \quad \textit{Outside sphere} \end{aligned} \quad (18)$$

In its general form the LAPW method expands the potential in the following form:

$$\begin{aligned} & V(\vec{r}) \\ &= \begin{cases} \sum_{lm} V_{lm}(\vec{r}) Y_{lm}(\hat{r}) & \textit{inside sphere} \\ \sum_{\vec{k}} V_{\vec{k}} e^{i\vec{k}\cdot\vec{r}} & \textit{outside sphere} \end{cases} \end{aligned} \quad (19)$$

Chapter Three

Results and Discussion

3.1 Computational Method

The full potential linearized augmented plane wave, implemented in WIEN2k^[28] package have been used to report the calculations in the present work. For the compound Co_2CrAl , the muffin-tin radii (R_{MT}) of Co, Cr and Al atoms are 2.1, 2.05 and 1.95 a.u., respectively and for the compound Cr_2MnSb , R_{MT} of Cr, Mn and Sb atoms are 2.14, 2.2 and 2.2 a.u., respectively. Moreover, there are 35 special k-points in the irreducible Brillion zone (IBZ) with grid $10 \times 10 \times 10$ (equivalent to 1000 k-points in the Full Brillion Zone (BZ))^[29] are used to obtain self-consistency for Co_2CrAl and Cr_2MnSb compounds. Also, the number of plane waves was restricted by $K_{MAX} R_{MT} = 8$ and the expansions of the wave functions was set by $l=10$ inside the muffin-tin spheres. However the self-consistent calculations are considered to converge only when the calculated total energy of the crystal converges to be less than 10^{-5} Ry. Also, the elastic constants of the cubic phase are calculated by using second-order derivative within formalism WIEN2k code.

3.2 Structural Properties

By fitting the total energy to Birch–Murnaghan’s equation of state (EOS),^[30] the optimized lattice constant (a), bulk modulus (B) and its pressure derivative (B’) were calculated. Birch–Murnaghan’s equation of state (EOS) is given by:

$$\mathbf{E}(\mathbf{V}) = \mathbf{E}_0 + \frac{9\mathbf{V}_0\mathbf{B}_0}{16} \left\{ \left[\left(\frac{\mathbf{V}_0}{\mathbf{V}} \right)^{\frac{2}{3}} - 1 \right]^3 \mathbf{B}_0' + \left[\left(\frac{\mathbf{V}_0}{\mathbf{V}} \right)^{\frac{2}{3}} - 1 \right]^2 \left[6 - 4 \left(\frac{\mathbf{V}_0}{\mathbf{V}} \right)^{\frac{2}{3}} \right] \right\} \quad (20)$$

$$\text{Pressure, } \mathbf{P} = - \frac{d\mathbf{E}}{d\mathbf{V}}, \text{ Bulk modulus, } \mathbf{B} = - \mathbf{V} \frac{d\mathbf{P}}{d\mathbf{V}} = \mathbf{V} \frac{d^2\mathbf{E}}{d\mathbf{V}^2}$$

Where B is the bulk modulus at the equilibrium volume, B’ is the pressure derivative of the bulk modulus at the equilibrium volume and E_0 is the minimum energy.

The normal Heusler Co_2CrAl and Cr_2MnSb compounds have space group Fm-3m L21 (225) and inverse Heusler Co_2CrAl and Cr_2MnSb compounds have space group F-43m X (216)^[31], while Tetragonal crystal lattices result from stretching a cubic lattice along one of its lattice vectors, so that the cube becomes a rectangular prism with a square base (a by a) and height (c, which is different from (a). Therefore, tetragonal Heusler Co_2CrAl and Cr_2MnSb compounds have space groups of I4/mmm (139) and I-4m2 (119). The structural properties for Full-Heusler Co_2CrAl and Cr_2MnSb compounds were calculated. The crystal structures of Full-Heusler Co_2CrAl and Cr_2MnSb compounds are shown in Figure 3. The total energy as function of the volume for Heusler Co_2CrAl and Cr_2MnSb compounds

are shown in Figures (4 and 5). Moreover the optimized structural parameters are calculated from the equation of state (EOS) and tabulated in Tables 1 and 2. Normally, almost all materials have a positive value of B' approximately 4.8. In other words, with increasing pressure, the values of their bulk moduli increased, indicating that the materials are not easily compressible. The presently observed negative value of B' implies a decrease in the bulk modulus with an increase in pressure. The anomalous compression must be a result of the pressure dependence of the c axis because the dependences of a and b axes are linear as shown in Table 2 for tetragonal Heusler Cr_2MnSb compound with space groups of $I4/mmm$ (139).

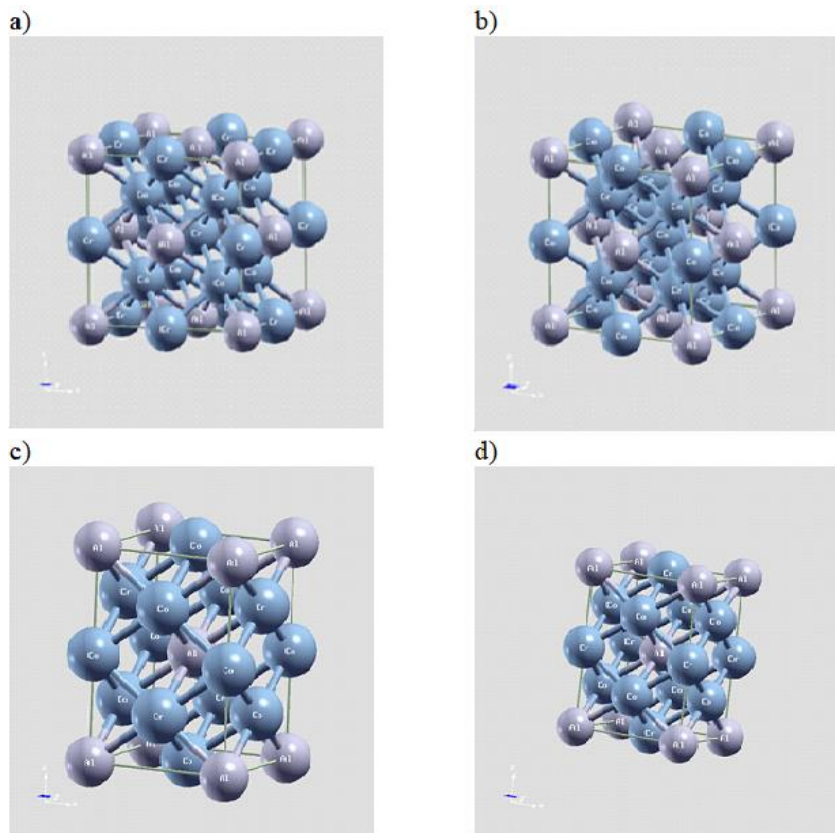


Figure 3: Different crystal structures of Heusler Co_2CrAl a) normal Heusler structure Co_2CrAl Fm-3m L21 (225), b) inverse Heusler Co_2CrAl structure F-43m X (216), c) Tetragonal structure $I4/mmm$ (139), d) Tetragonal structure $I-4m2$ (119).

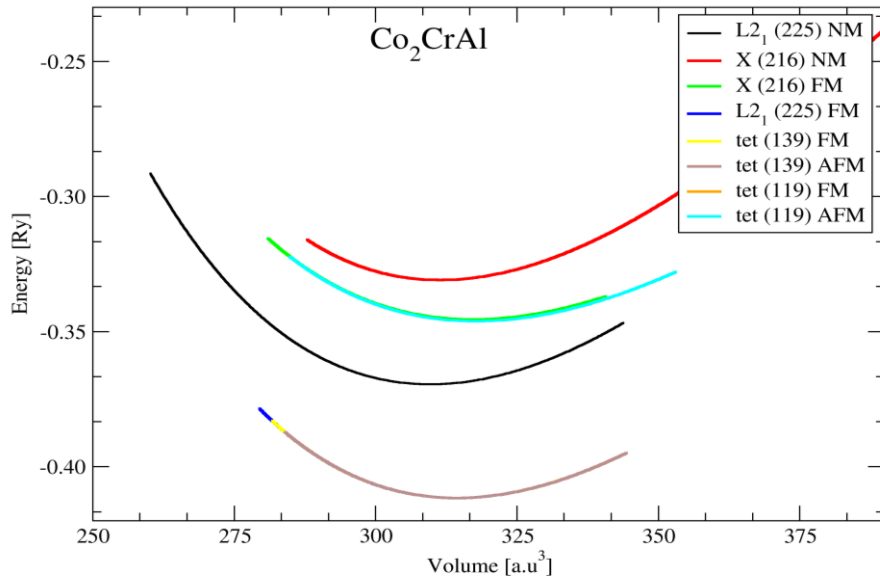


Figure 4: The total energy (Ry) versus volume (a.u.^3) for different crystal structure of Co_2CrAl Heusler.

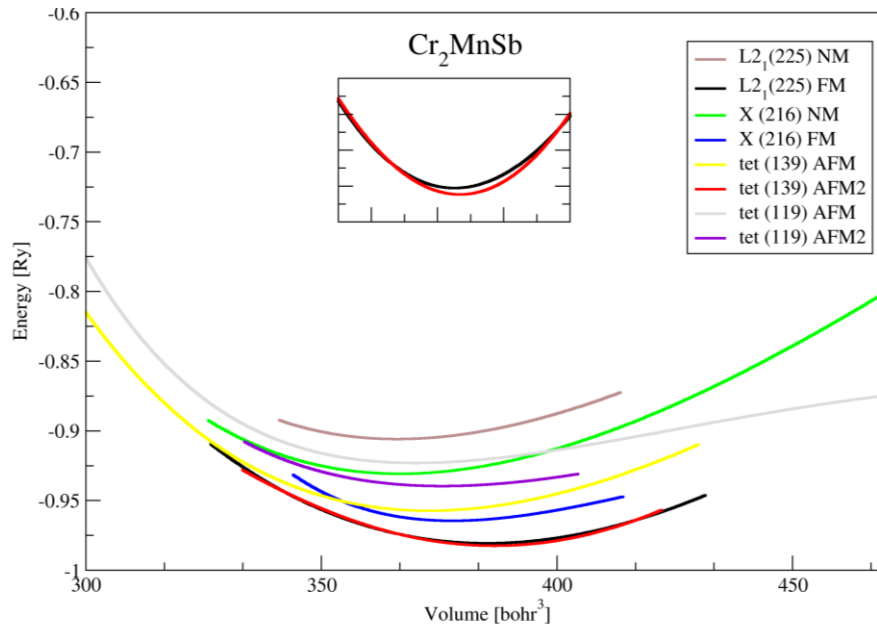


Figure 5: The total energy (Ry) versus volume (a.u.^3) for different crystal structures of Cr_2MnSb Heusler.

The lattice parameter (a), bulk modulus (B), first pressure derivative of the Bulk modulus (B') and total energy are tabulated in Tables 1 and 2:

Table 1: Calculated lattice parameter (a), bulk modulus (B), first pressure derivative of the Bulk modulus (B'), c/a and total energy for Heusler Co_2CrAl compound.

Structure	Space group	Magnetic phase	Reference	Lattice parameter a (\AA)	B (GPa)	B' (GPa)	E_{total} (Ry)/f.u	c/a
Co_2CrAl	Normal Fm-3m (225)	NM	Present	5.6830	213.468	4.28138	-8161.3694	1
	Normal Fm-3m (225)	FM	Present	5.7082	206.8110	5.3119	-8161.4115	1
			Experimental	5.73 ^[19]				
			Theoretical	5.74 ^[19]				
	Inverse F-43m (216)	NM	Present	5.6936	212.056	4.7616	-8161.3309	1
	Inverse F-43m (216)	FM	Present	5.7398	169.0397	5.479	-8161.3454	1
	I4/mmm (139)	FM	Present	4.011	202.24	4.472	-8161.41148	1.4175
	I4/mmm (139)	AFM	Present	4.0239	202.133	4.508	-8161.4095	1.4175
	I-4m2 (119)	FM	Present	3.9382	166.847	4.776	-8161.34608	1.5253
I-4m2 (119)	AFM	Present	3.9441	163.781	4.777	-8161.3458	1.5253	

Table 2: Calculated lattice parameter (a), bulk modulus (B), first pressure derivative of the Bulk modulus (B'), c/a and total energy for Heusler Cr_2MnSb compound.

Structure	Space group	Magnetic phase	Reference	Lattice parameter a (\AA)	B (GPa)	B' (GPa)	E_{total} (Ry)/f.u	c/a
Cr_2MnSb	Normal Fm-3m (225)	NM	Present	6.1116	201.77	1.797	-19487.9803	1
	Normal Fm-3m (225)	FM	Present	6.1381	248.45	5.2958	-19487.98197	1
			Other method	6.1 ^[21]				
	Inverse F-43m (216)	NM	Present	6.0724	220.322	11.6629	-19487.9644	1
	Inverse F-43m (216)	FM	Present	6.0571	149.5381	6.6223	-19487.9683	1
			Other method	6.1 ^[21]				
	I4/mmm (139)	FM	Present	4.3337	296.852	- 9.455	-19487.982	1.4158
	I4/mmm (139)	AFM	Present	4.2637	386.728	20.301	-19487.9823	1.4158
I-4m2 (119)	FM	Present	4.0617	142.459	7.538	-19487.9394	1.6513	
I-4m2 (119)	AFM	Present	4.0459	153.8705	10.616	-19487.9394	1.6513	

Tables 1 and 2 show that our calculated lattice parameters are in good agreement with the experimental lattice parameters of normal and inverse Heusler Co_2CrAl , Cr_2MnSb compounds. The calculated lattice parameters for normal Heusler Co_2CrAl compound are slightly underestimated the experimental lattice parameter with 0.55% ^[19]. On the other hand, the calculated lattice parameters for normal and inverse Heusler Cr_2MnSb compound are slightly underestimated the experimental lattice parameter with 0.70% ^[21] smaller for inverse and overestimated the experimental lattice parameter with 0.62% ^[21] larger for normal.

Our volume optimization results shown that the AFM tetragonal distortion (no. 139) is more preferred than the FM cubic $L2_1$ for Cr_2MnSb with a slightly small energy difference $\Delta E_{tet-cubic} = 0.0047 \frac{Ry}{f.u}$ from equation 21, whereas the FM cubic $L2_1$ is more preferred than tetragonal distortion for the Co_2CrAl case with energy difference $\Delta E_{tet-cubic} = 0.002 \frac{Ry}{f.u}$. But to make the AFM tetragonal phase stable the energy difference with cubic structure should be greater than $0.1 eV/f.u$. So as reported previously, Cr_2MnSb crystallize in cubic $L2_1$ structure with fully compensated ferrimagnetic configuration where magnetic moment of Cr and Mn are antiparallel exchange ^[21].

$$\Delta E_{tet-cubic} = E_{tet} - E_{cubic} \quad (21)$$

3.3 Magnetic Properties

In this part, we have calculated the total and partial magnetic moment for inverse, normal and tetragonal I4/mmm (139) Heusler Co_2CrAl , Cr_2MnSb compounds, and also compared the results with other experimental and theoretical works as shown in Tables 3 and 4. We have found that the normal and tetragonal Heusler Co_2CrAl are ferromagnetic compounds. On the other hand, the total magnetic moment for inverse Co_2CrAl compound is $M^{tot} = 0.83116(\mu_B)$. Therefore, present results show that the calculated total magnetic moment of normal Co_2CrAl compound are in excellent agreement with the experimental result^[19] and overestimated the theoretical value with 1.35% higher^[31] as shown in Table 3. When the total magnetic moment (M^{tot}) is integer value that means it is a half-metallic material.

Table 3: Total magnetic moment for inverse, normal and tetragonal I4/mmm (139) Heusler Co_2CrAl compounds.

Compounds		Magnetic Moment (μ_B)					
		Co	Co	Cr	Al	Interstitial	Total magnetic moment (M^{tot}) μ_B
Inverse Co_2CrAl	Present	0.96069	1.36311	-1.26906	-0.00841	-0.21497	0.83116
	Experimental Result	0.650 ^[19]	0.650 ^[19]	1.745 ^[19]	-0.045 ^[19]	–	3 ^[19]
Normal Co_2CrAl	Present	1.01815	1.01815	1.32570	-0.06082	-0.30118	3
	Theoretical Result	–	–	–	–	–	2.96 ^[32]
Tetragonal I4/mmm (139) Co_2CrAl	Present	-0.04084	-0.04084	0.81717	1.45741	-0.05097	2.99994

Table 4 shows the results for inverse, normal and tetragonal I4/mmm (139) Heusler Cr_2MnSb compound. Table 4 shows that the inverse Heusler Cr_2MnSb has negative spin moment for both Cr & Mn atoms and positive spin-moment for the second atom of Cr. The normal Heusler Cr_2MnSb has negative spin moment for Cr atoms and positive spin moment for Mn atom. While, the spin moment of the Sb atoms is very small in both structural types of Cr_2MnSb . Cr and Mn atoms have only one electron difference and similar electronic properties. Thus their exchange keeps the ferromagnetic character of the compounds resulting in small variations of the spin moments per site. We have found that the normal Heusler Cr_2MnSb

has small total magnetic moment which means that the normal Heusler Cr_2MnSb is a ferrimagnet. On the other hand, we have found that the inverse Heusler Cr_2MnSb has zero total magnetic moment which means that this compound is antiferromagnetic and the tetragonal Cr_2MnSb has small total magnetic moment which means that this compound is a ferrimagnet.

Table 4: Total magnetic moment for inverse, normal and tetragonal I4/mmm (139) Heusler Cr_2MnSb compounds.

Compounds		Magnetic Moment (μ_B)					Total magnetic moment (M^{tot}) μ_B
		Cr	Cr	Mn	Sb	Interstitial	
Inverse Cr_2MnSb	Present	-1.72053	2.68899	-1.05810	0.04777	0.04187	0
	Other method	1.96 ^[21]	-3.18 ^[21]	1.29 ^[21]	-	-	0 ^[21]
Normal Cr_2MnSb	Present	-1.51854	-1.51854	3.21064	0.06167	-0.23513	0.00011
	Other method	1.77 ^[21]	1.77 ^[21]	-3.44 ^[21]	-	-	0.01 ^[21]
Tetragonal I4/mmm (139) Cr_2MnSb	Present	0.05294	0.05294	-1.46141	3.08253	-0.20953	0.00312

3.4 Electronic Properties

In this part, the total and partial density of states, the band structure for normal and inverse Heusler (Co_2CrAl , Cr_2MnSb) compounds were investigated. It is clear from the band structure and density of states that normal Co_2CrAl , normal Cr_2MnSb and inverse Cr_2MnSb Heusler compounds have a half-metallic behavior in the ferromagnetic state, that means at spin up the materials behave as metallic nature while at spin down the materials behave as semiconducting nature, while the inverse Heusler Co_2CrAl compound has metallic behavior. Whereas, the Tetragonal I4/mmm (139) Heusler (Co_2CrAl , Cr_2MnSb) compounds have a half-metallic behavior in the antiferromagnetic state.

Figure 6 (a and b) shows metallic behavior of the spin up and spin down band structures within pBE-GGA method for inverse Heusler Co_2CrAl compound with zero energy gap. Also, Figure 7 (a and b) shows metallic behavior of the spin up and spin down band structures within mBJ-GGA method for inverse Heusler Co_2CrAl compound with zero energy gap.

Figure 8 (a and b) shows that the band structure spin down of normal Heusler Co_2CrAl compound has an indirect energy band gap using PBE-GGA method. Also, Figure 9 (a and b) shows that the band structure spin down of normal Heusler Co_2CrAl compound has an indirect energy band gap using mBJ-GGA method. The indirect energy gaps within PBE-GGA and mBJ-GGA found to be 0.6 eV, 0.9 eV respectively, as shown in Table 5. Figure 10 (a and b) shows that the band structure spin down of inverse

Heusler Cr_2MnSb compound has an indirect energy band gap using PBE-GGA method. Also, Figure 11 (a and b) shows that the band structure spin down of inverse Heusler Cr_2MnSb compound has an indirect energy band gap using mBJ-GGA method. The indirect energy gaps within PBE-GGA and mBJ-GGA found to be 0.9 eV, 1 eV respectively, as shown in Table 6.

Figure 12 (a and b) shows that the band structure spin down of normal Heusler Cr_2MnSb compound has an indirect energy band gap using PBE-GGA method. Also, Figure 13 (a and b) shows that the band structure spin down of normal Heusler Cr_2MnSb compound has an indirect energy band gap using mBJ-GGA method. The indirect energy gaps within PBE-GGA and mBJ-GGA found to be 0.8 eV, 0.9 eV respectively, as shown in Table

6. Figure 14 (a and b) shows the band structure for Tetragonal I4/mmm (139) Heusler Co_2CrAl compound in AFM state. Figure 14a shows that the spin up band structure of Tetragonal I4/mmm (139) Heusler Co_2CrAl compound has metallic nature, while Figure 14b shows that the spin down band structure of Tetragonal I4/mmm (139) Heusler Co_2CrAl compound has direct energy band gap. The direct energy gap found to be 0.8 eV as shown in Table 7. Figure 15 (a and b) shows the band structure for Tetragonal I4/mmm (139) Heusler Cr_2MnSb compound in AFM state. Figure 15a shows that the spin up band structure of Tetragonal I4/mmm (139) Heusler Cr_2MnSb compound has metallic nature, while Figure 15b shows that the spin down band structure of Tetragonal I4/mmm (139) Heusler Cr_2MnSb compound has direct energy band gap. The direct energy gap found to be 0.9 eV as shown in Table 7.

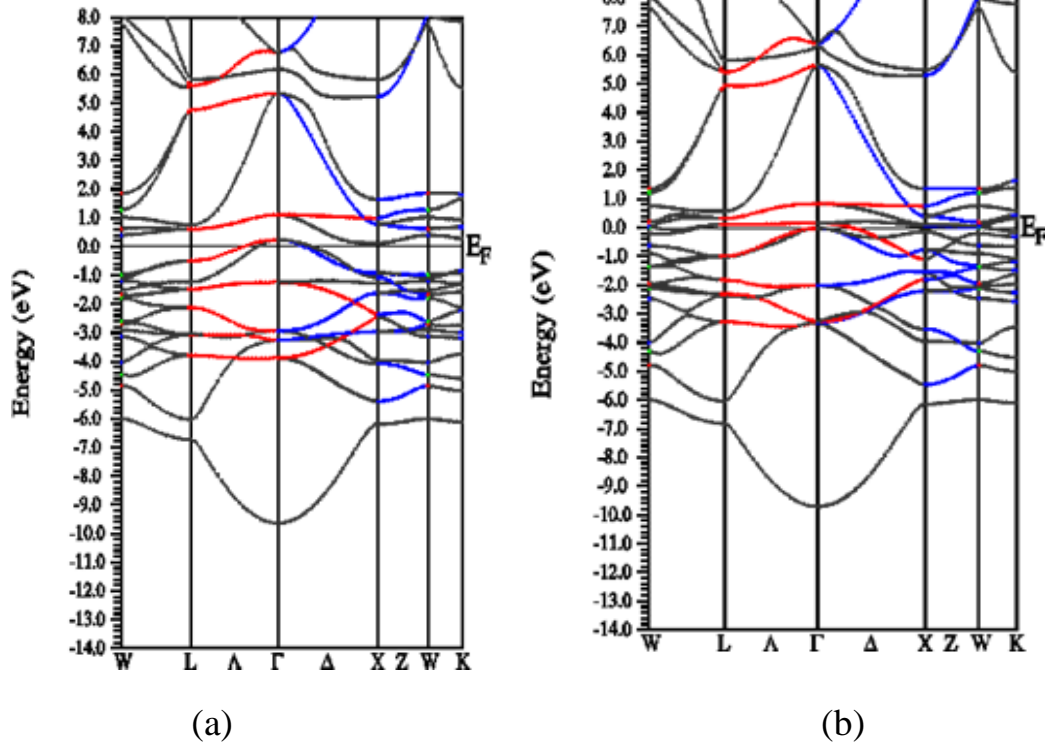


Figure 6: The band structure for inverse Heusler Co_2CrAl compound by using PBE-GGA method for (a) spin up inverse Heusler Co_2CrAl compound (b) spin down inverse Heusler Co_2CrAl compound.

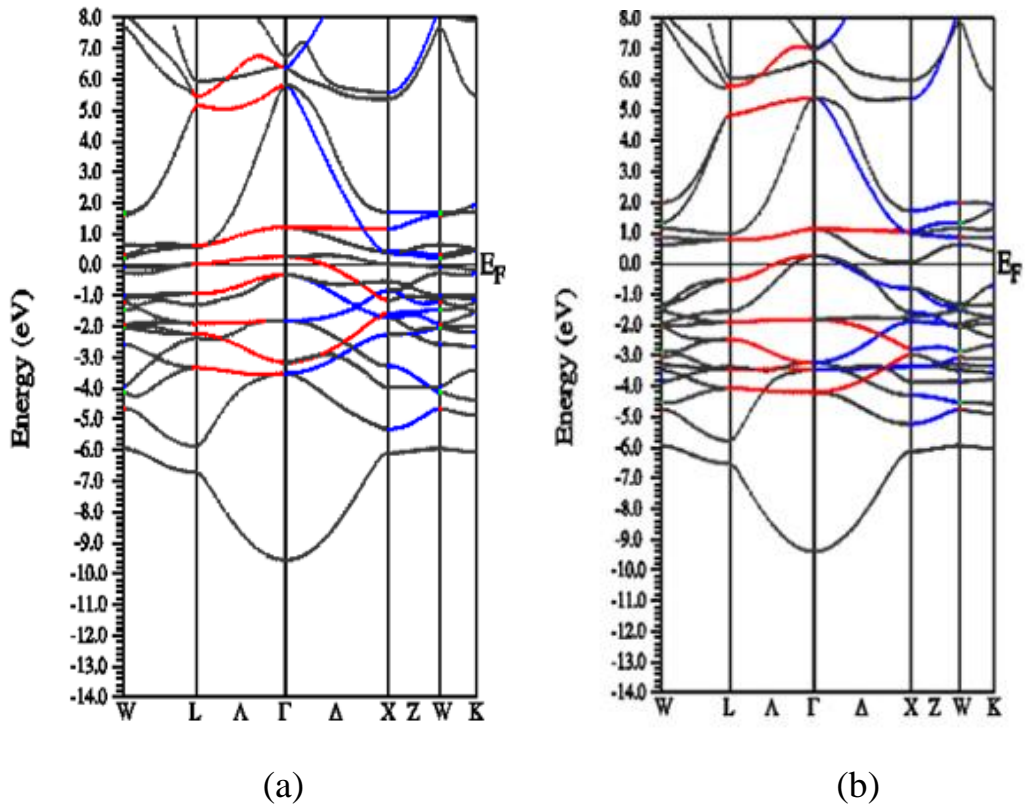
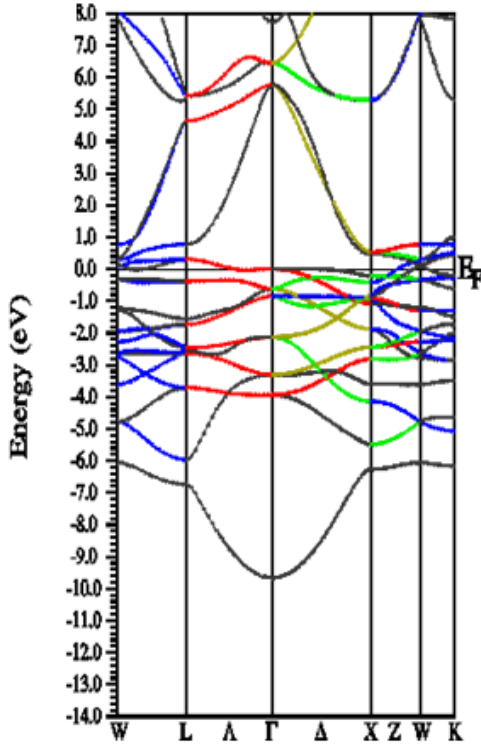
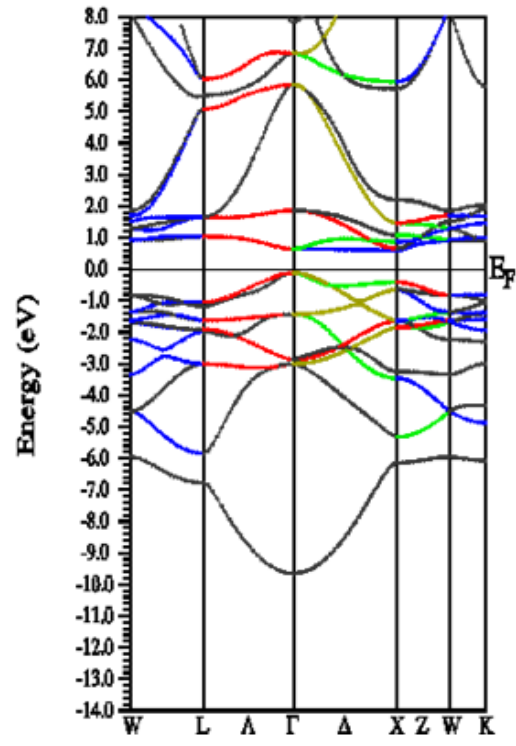


Figure 7: The band structure for inverse Heusler Co_2CrAl compound by using mBJ-GGA method for (a) spin up inverse Heusler Co_2CrAl compound (b) spin down inverse Heusler Co_2CrAl compound.

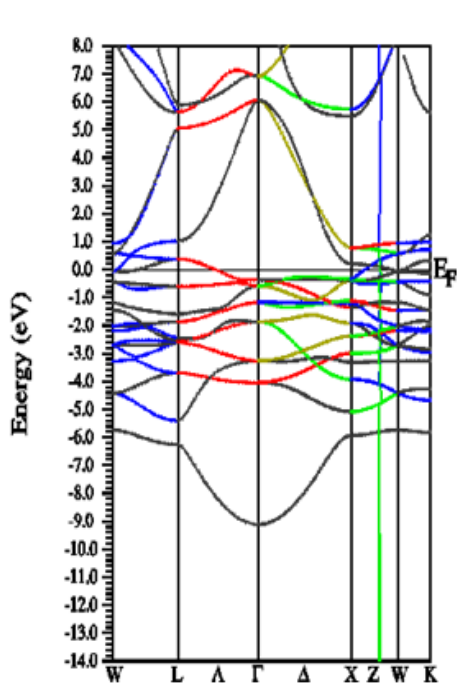


(a)

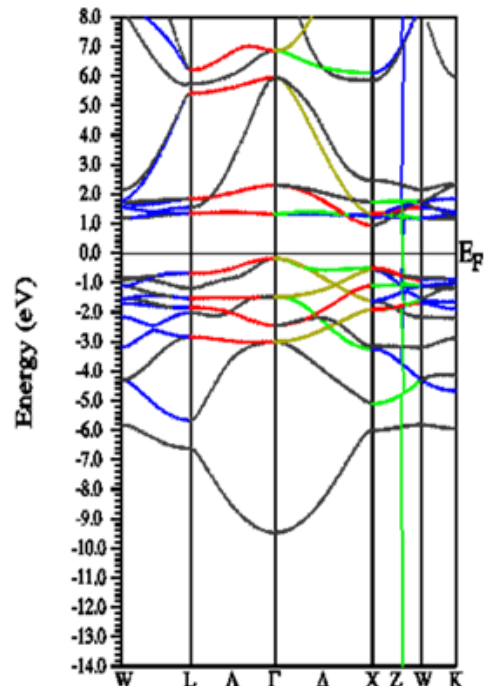


(b)

Figure 8: The band structure for normal Heusler Co_2CrAl compound by using PBE-GGA method for (a) spin up normal Heusler Co_2CrAl compound (b) spin down normal Heusler Co_2CrAl compound.



(a)



(b)

Figure 9: The band structure for normal Heusler Co_2CrAl compound by using mBJ-GGA method for (a) spin up normal Heusler Co_2CrAl compound (b) spin down normal Heusler Co_2CrAl compound.

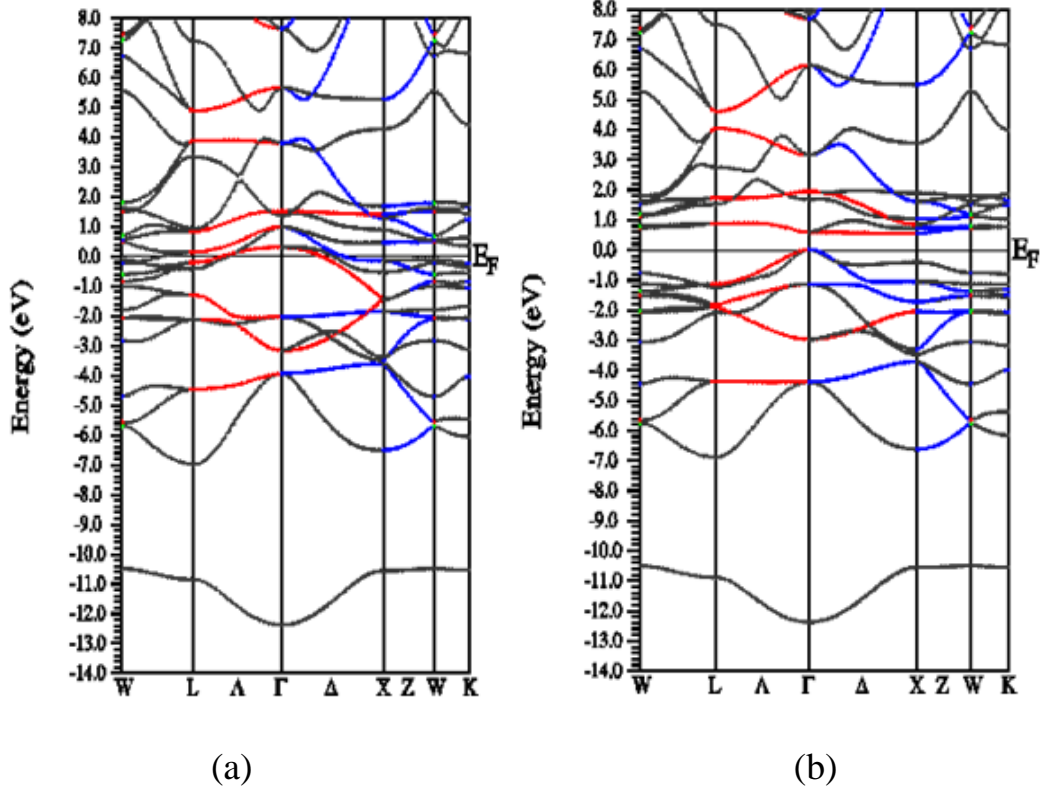


Figure 10: The band structure for inverse Heusler Cr_2MnSb compound by using PBE-GGA method for (a) spin up inverse Heusler Cr_2MnSb compound (b) spin down inverse Heusler Cr_2MnSb compound.

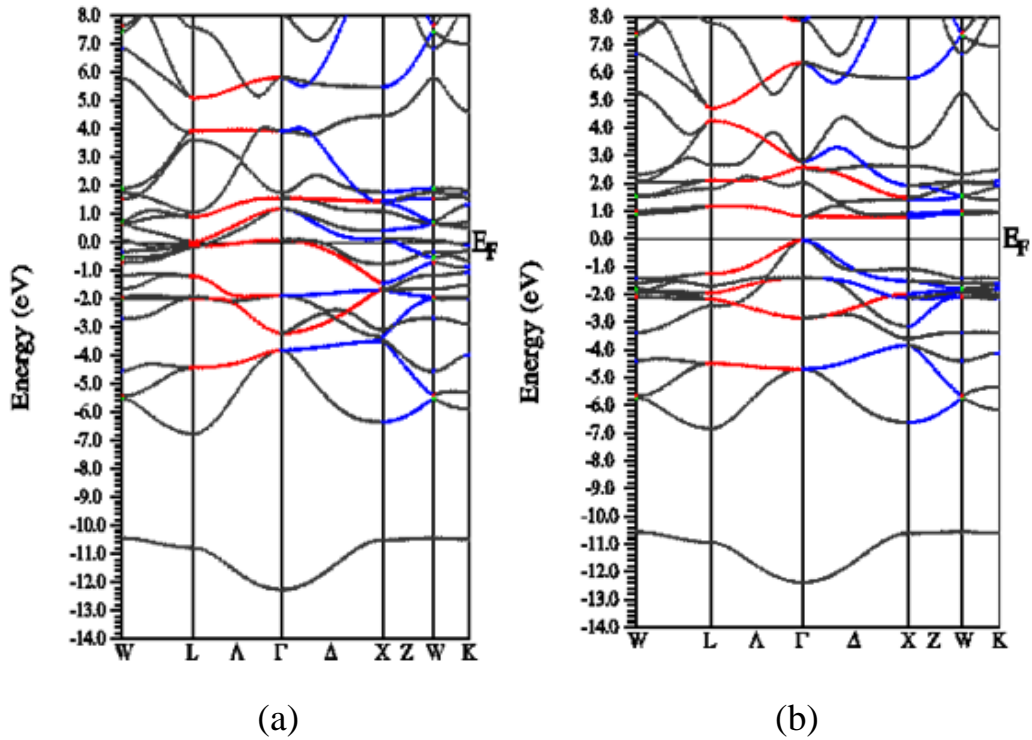


Figure 11: The band structure for inverse Heusler Cr_2MnSb compound by using mBJ-GGA method for (a) spin up inverse Heusler Cr_2MnSb compound (b) spin down inverse Heusler Cr_2MnSb compound.

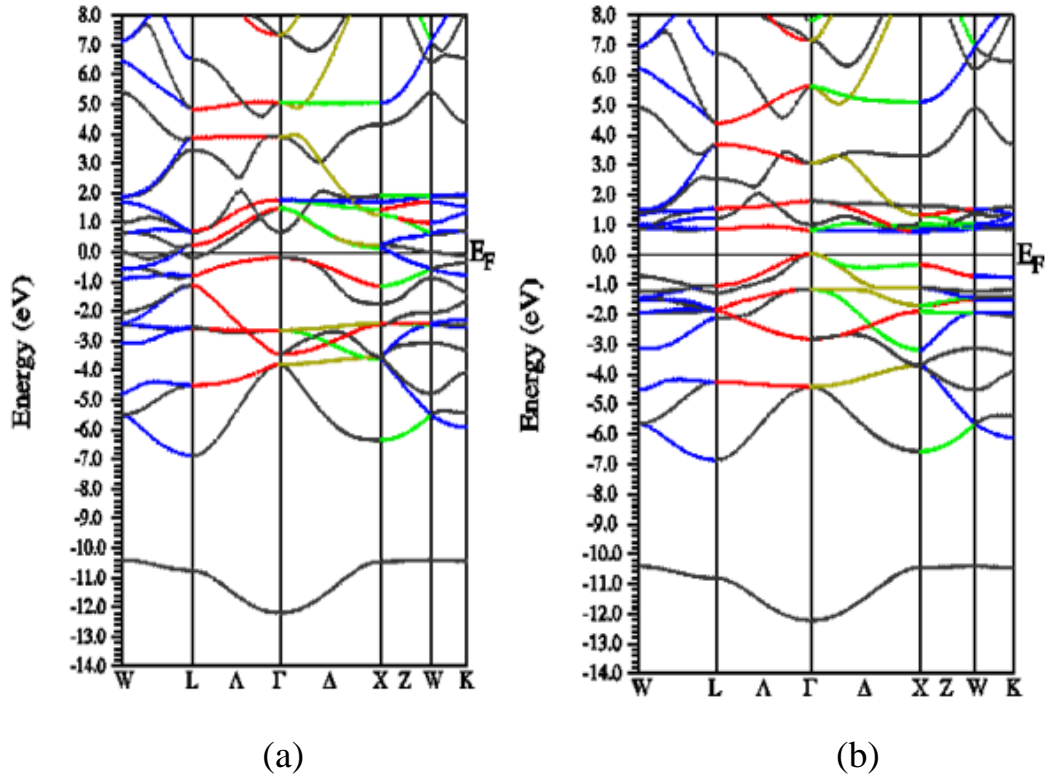


Figure 12: The band structure for normal Heusler Cr_2MnSb compound by using PBE-GGA method for (a) spin up normal Heusler Cr_2MnSb compound (b) spin down normal Heusler Cr_2MnSb compound.

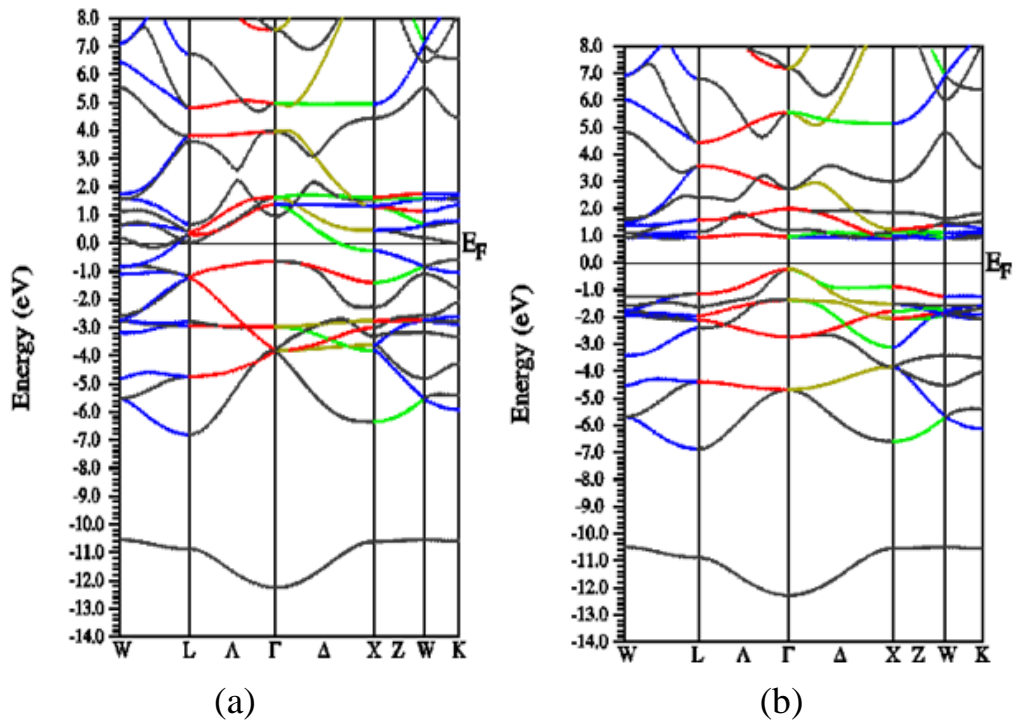


Figure 13: The band structure for normal Heusler Cr_2MnSb compound by using mBJ-GGA method for (a) spin up normal Heusler Cr_2MnSb compound (b) spin down normal Heusler Cr_2MnSb compound.

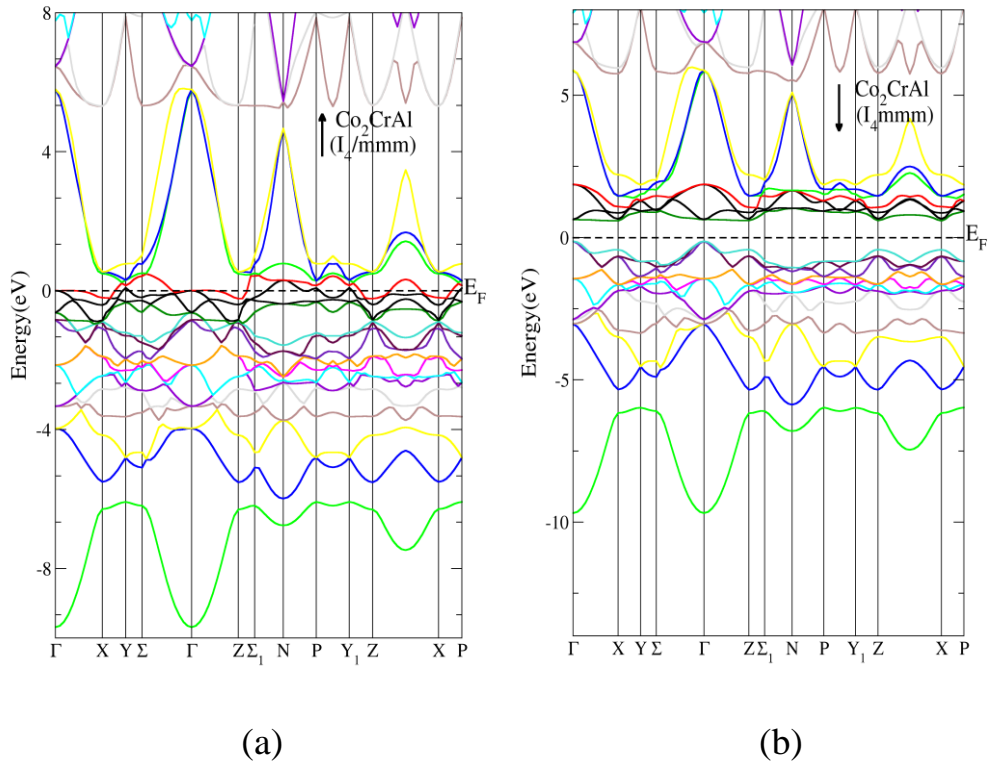


Figure 14: The band structure for Tetragonal I_4/mmm (139) Heusler Co_2CrAl compound in AFM state (a) spin up Tetragonal I_4/mmm Heusler (139) Co_2CrAl compound (b) spin down Tetragonal I_4/mmm Heusler (139) Co_2CrAl compound.

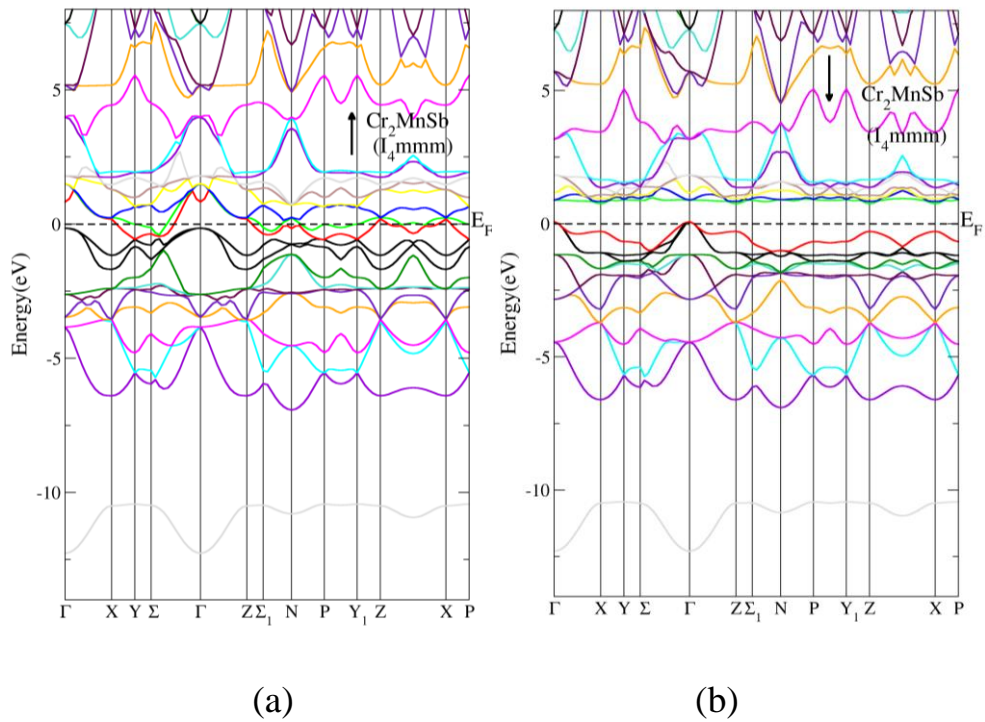


Figure 15: The band structure for Tetragonal I_4/mmm (139) Heusler Cr_2MnSb compound in AFM state (a) spin up Tetragonal I_4/mmm Heusler (139) Cr_2MnSb compound (b) spin down Tetragonal I_4/mmm Heusler (139) Cr_2MnSb compound.

Table 5: Energy band gaps for normal and inverse Co_2CrAl compound using PBE-GGA and mBJ methods.

Compounds	Band gap type	High Symmetry Lines	E_g -PBE-GGA (eV)	E_g -mBJ-GGA (eV)
<i>Normal</i> – Co_2CrAl	Indirect	$\Gamma - X$	0.6	0.9
<i>Inverse</i> – Co_2CrAl	Metallic	-	-	-

Table 6: Energy band gaps for normal and inverse Cr_2MnSb compound using PBE-GGA and mBJ methods.

Compounds	Band gap type	High Symmetry Lines	E_g -PBE-GGA (eV)	E_g -mBJ-GGA (eV)
Normal- Cr_2MnSb	Direct	Γ	0.9	1
Inverse- Cr_2MnSb	Direct	Γ	0.8	0.9

Table 7: Energy band gaps for Tetragonal I4/mmm (139) Heusler (Co_2CrAl , Cr_2MnSb) compounds in AFM state.

Compounds	Band gap type	High Symmetry Lines	E_g (eV)
Co_2CrAl	Direct	Γ	0.8
Cr_2MnSb	Direct	Γ	0.9

Figures 16-23 show the total and partial density of states for spin-up and spin-down for normal and inverse Heusler (Co_2CrAl , Cr_2MnSb) compounds. Density of states in Figures 16-23 show also half metallic behavior for normal Heusler Co_2CrAl , inverse and normal Heusler Cr_2MnSb compound with existing small energy band gap in spin down direction, this means that these compounds have half- metallic behavior.

In the spin-up of normal Co_2CrAl (Figure 18), the valence band is due to the d-state of Co, d-state of Cr and small contribution from Al s-state. Therefore, the conduction band is due to d-state of Co, d-state of Cr and small contribution from Al s-state. In spin-down of normal Co_2CrAl (Figure 19), the valence band is due to the d-state of Co, d-state of Cr and small contribution from Al s-state, while the conduction band is due to d-state of Co, d-state of Cr and small contribution from Al s-state.

In the spin-up of inverse Cr_2MnSb (Figure 20), the valence band is due to the d-state of Cr, d-state of Mn, s-state and p-state of Sb, while the conduction band is due to d-state of Cr, d-state of Mn, small contribution from s-state and p-state of Sb. In spin-down of inverse Cr_2MnSb (Figure 21), the valence band is due to the small contribution of d-state of Cr, d-state of Mn, s-state and p-state of Sb, while the conduction band is due to d-state of Cr, d-state of Mn, small contribution of s-state and p-state of Sb.

In the spin-up of normal Cr_2MnSb (Figure 22), the valence band is due to the d-state of Cr, d-state of Mn, s-state and p-state of Sb, while the conduction band is due to d-state of Cr, small contribution of s-state and p-state of Sb. In the spin-down of normal Cr_2MnSb (Figure 23), the valence band is due to the d-state of Cr, d-state of Mn, s-state and p-state of Sb, while the conduction band is due to d-state of Cr, small contribution from s-state and p-state of Sb.

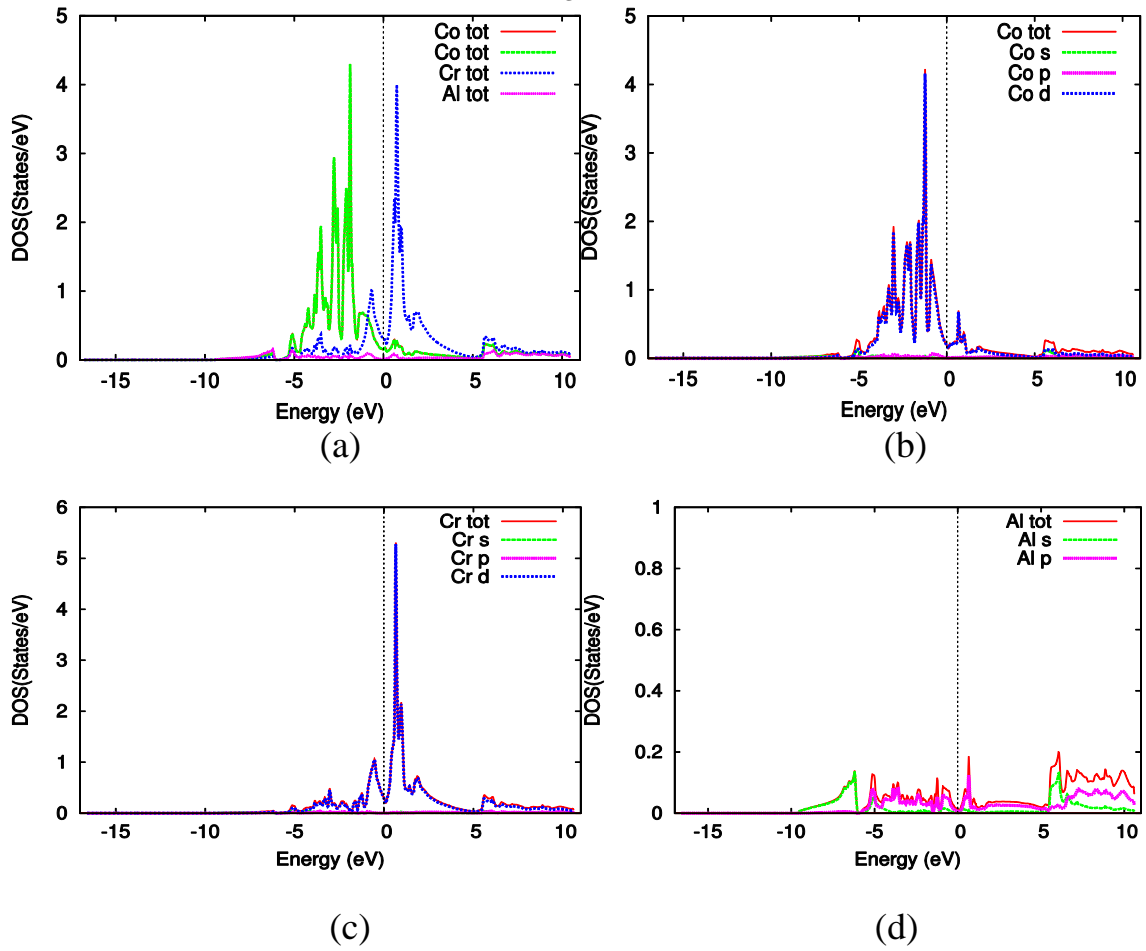


Figure 16: (a) Total density of states of spin up for inverse Co_2CrAl and partial density of states of spin up for (b) Co atom (c) Cr atom (d) Al atom of inverse Co_2CrAl compound.

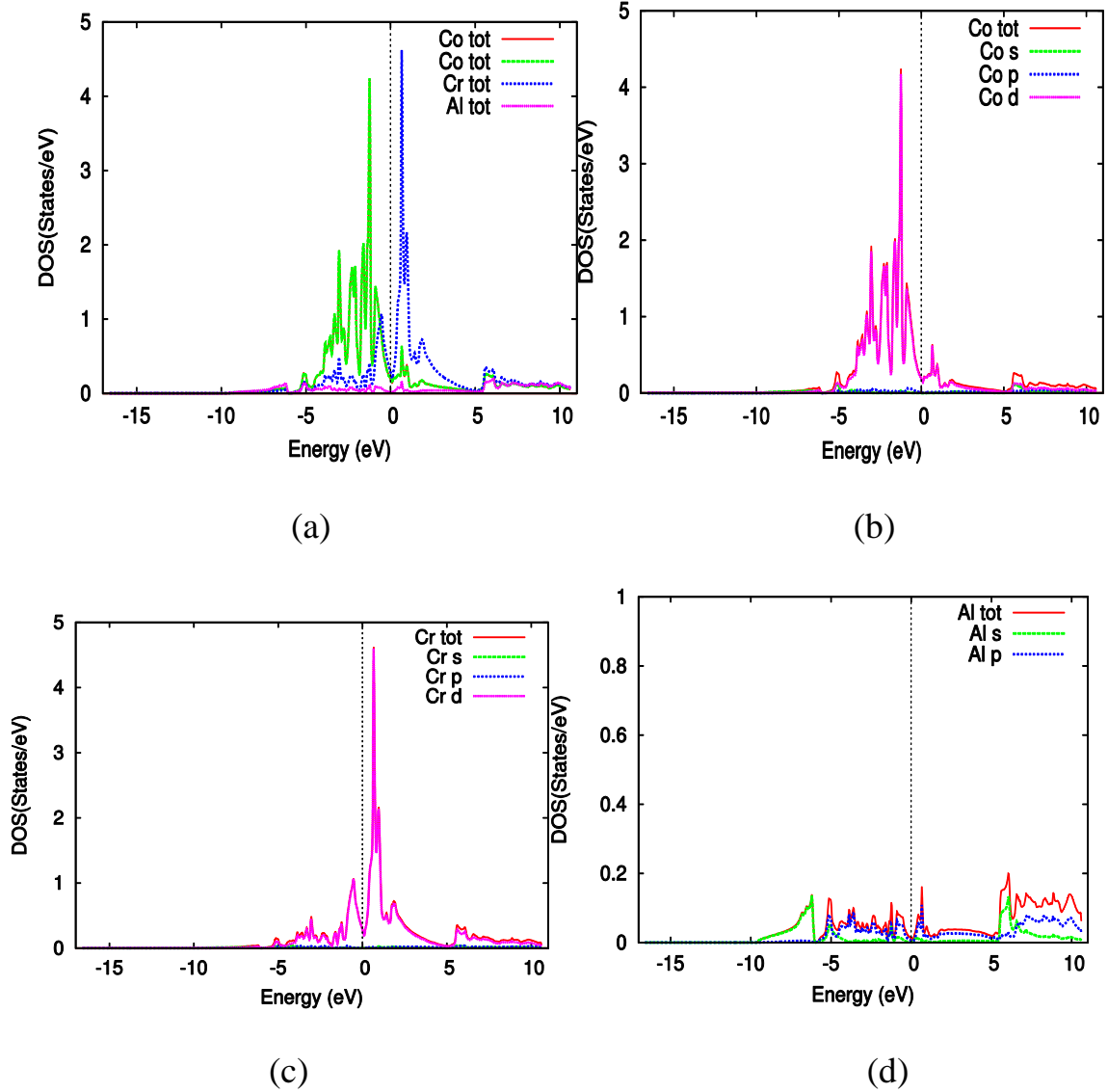


Figure 17: (a) Total density of states of spin down for inverse Co_2CrAl and partial density of states of spin up for (b) Co atom (c) Cr atom (d) Al atom of inverse Co_2CrAl compound.

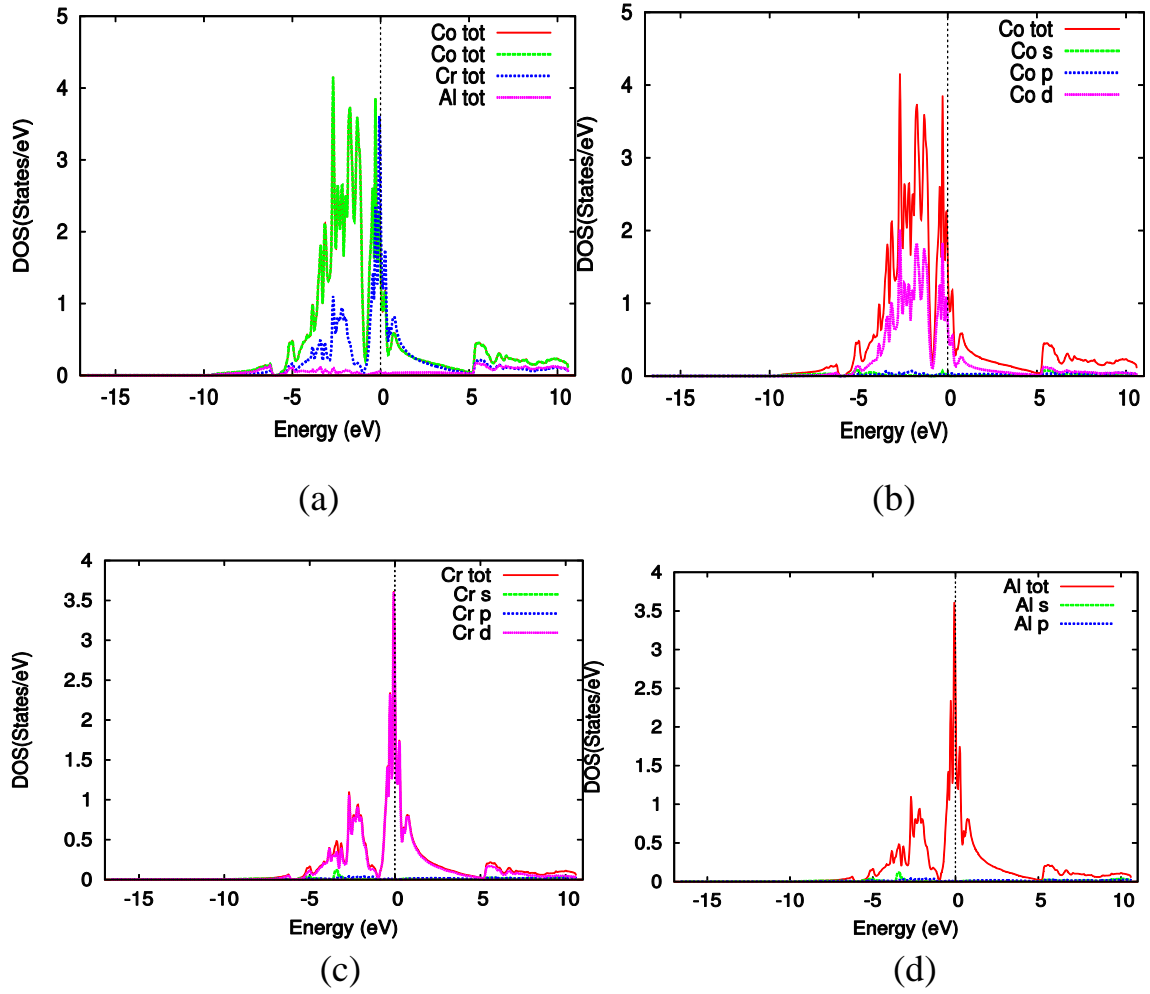


Figure 18: (a) Total density of states of spin up for normal Co_2CrAl and partial density of states of spin up for (b) Co atom (c) Cr atom (d) Al atom of normal Co_2CrAl compound.

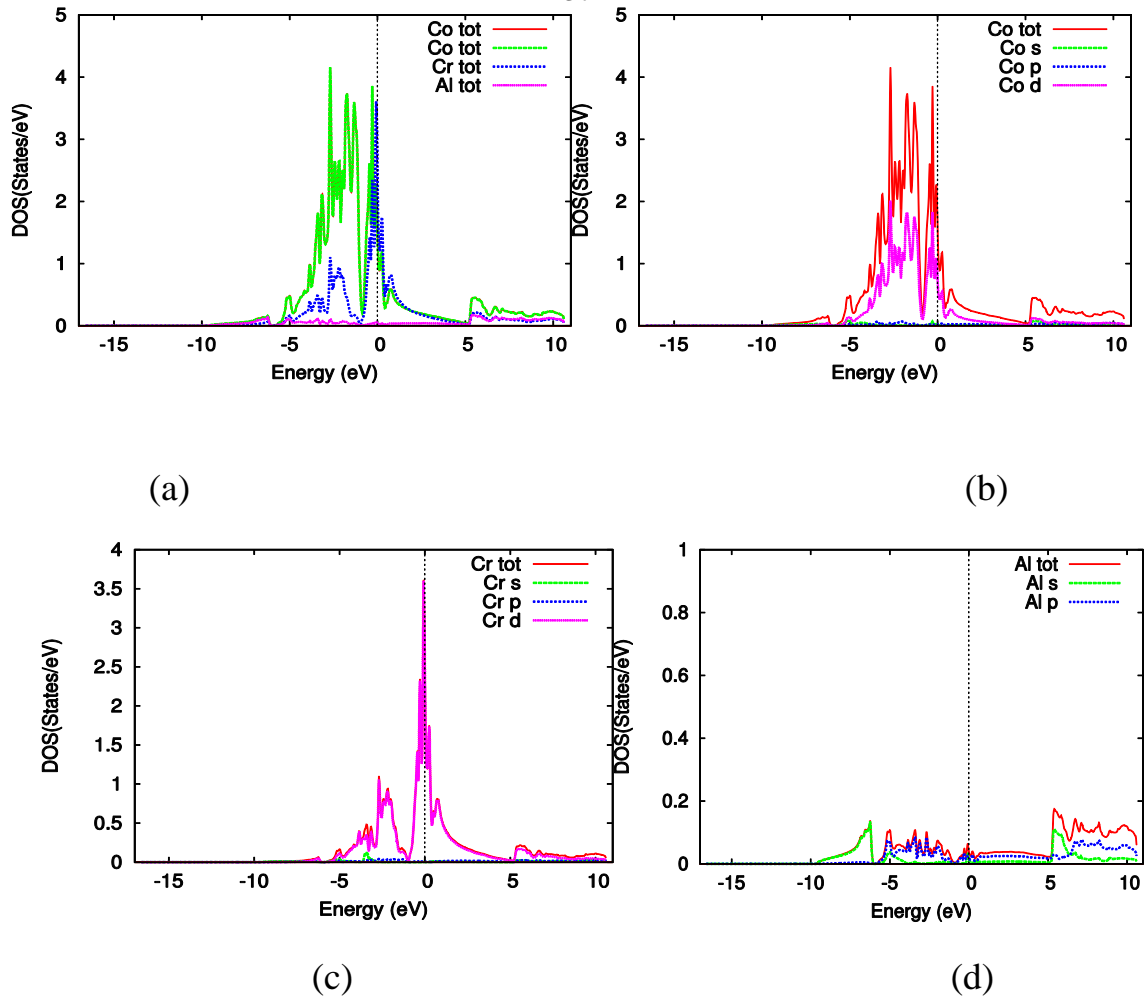


Figure 19: (a) Total density of states of spin down for normal Co_2CrAl and partial density of states of spin up for (b) Co atom (c) Cr atom (d) Al atom of normal Co_2CrAl compound.

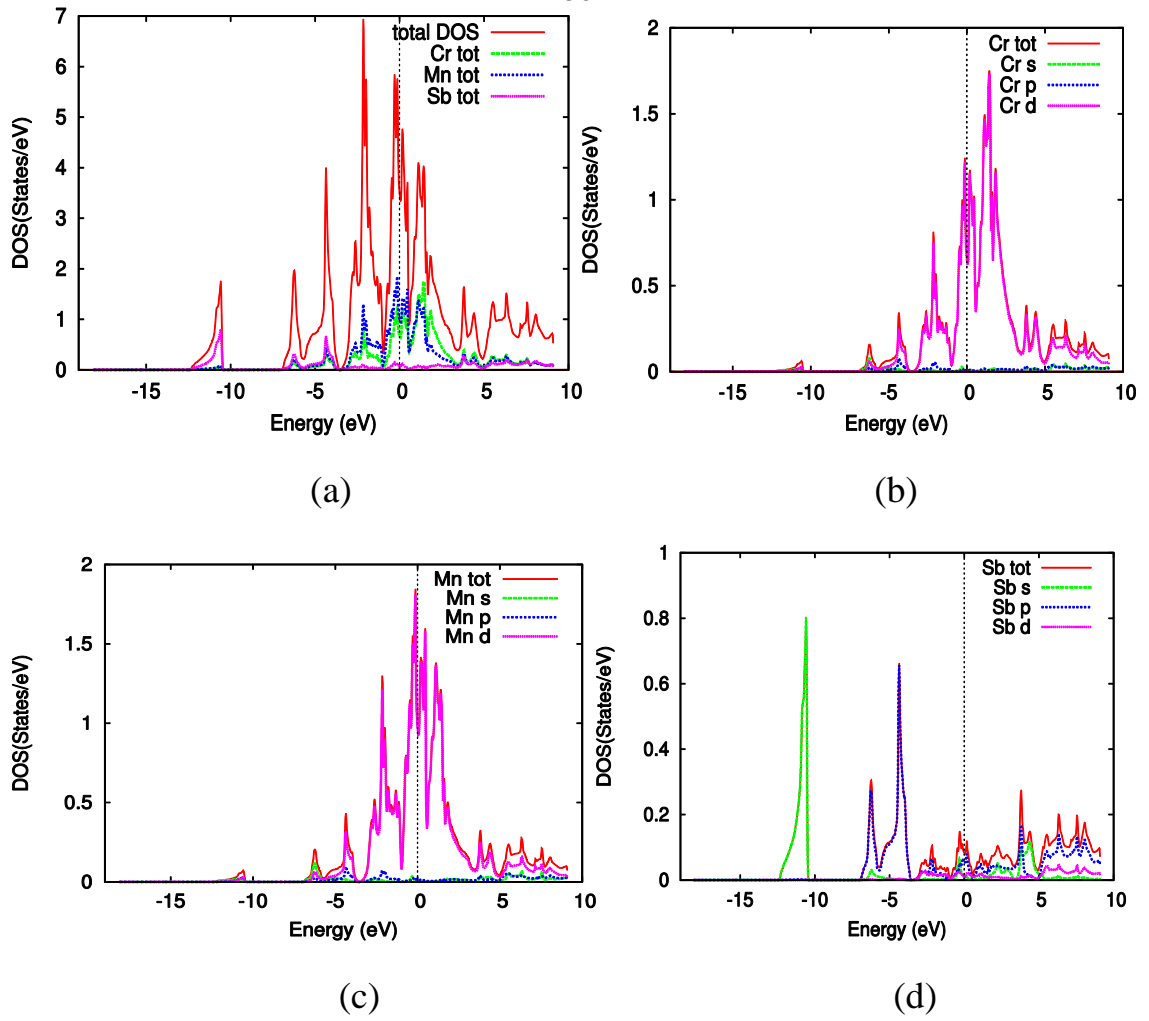


Figure 20: (a) Total density of states of spin up for inverse Cr_2MnSb and partial density of states of spin up for (b) Cr atom (c) Mn atom (d) Sb atom of inverse Cr_2MnSb compound.

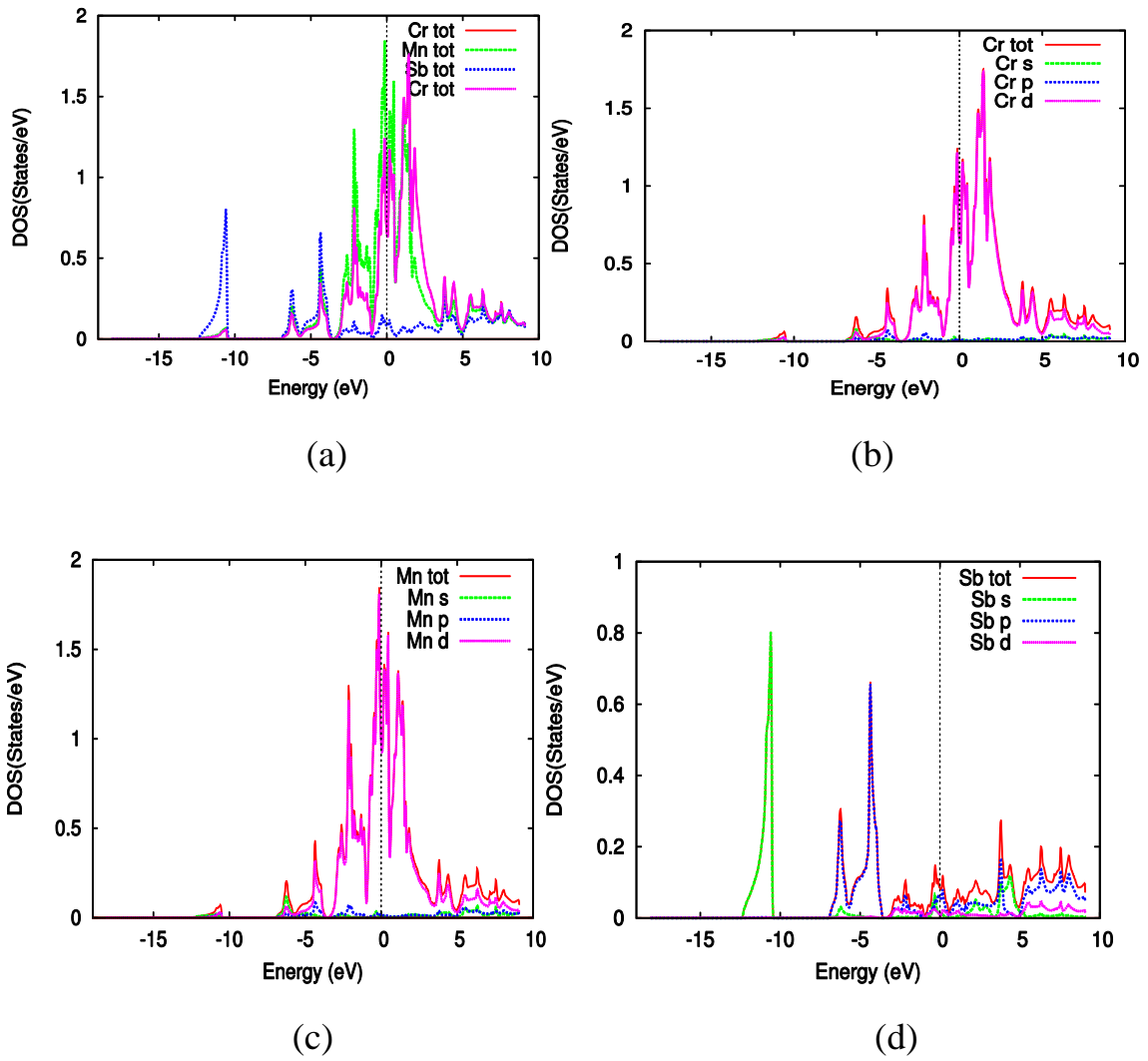


Figure 21: (a) Total density of states of spin down for inverse Cr_2MnSb and partial density of states of spin up for (b) Cr atom (c) Mn atom (d) Sb atom of inverse Cr_2MnSb compound.

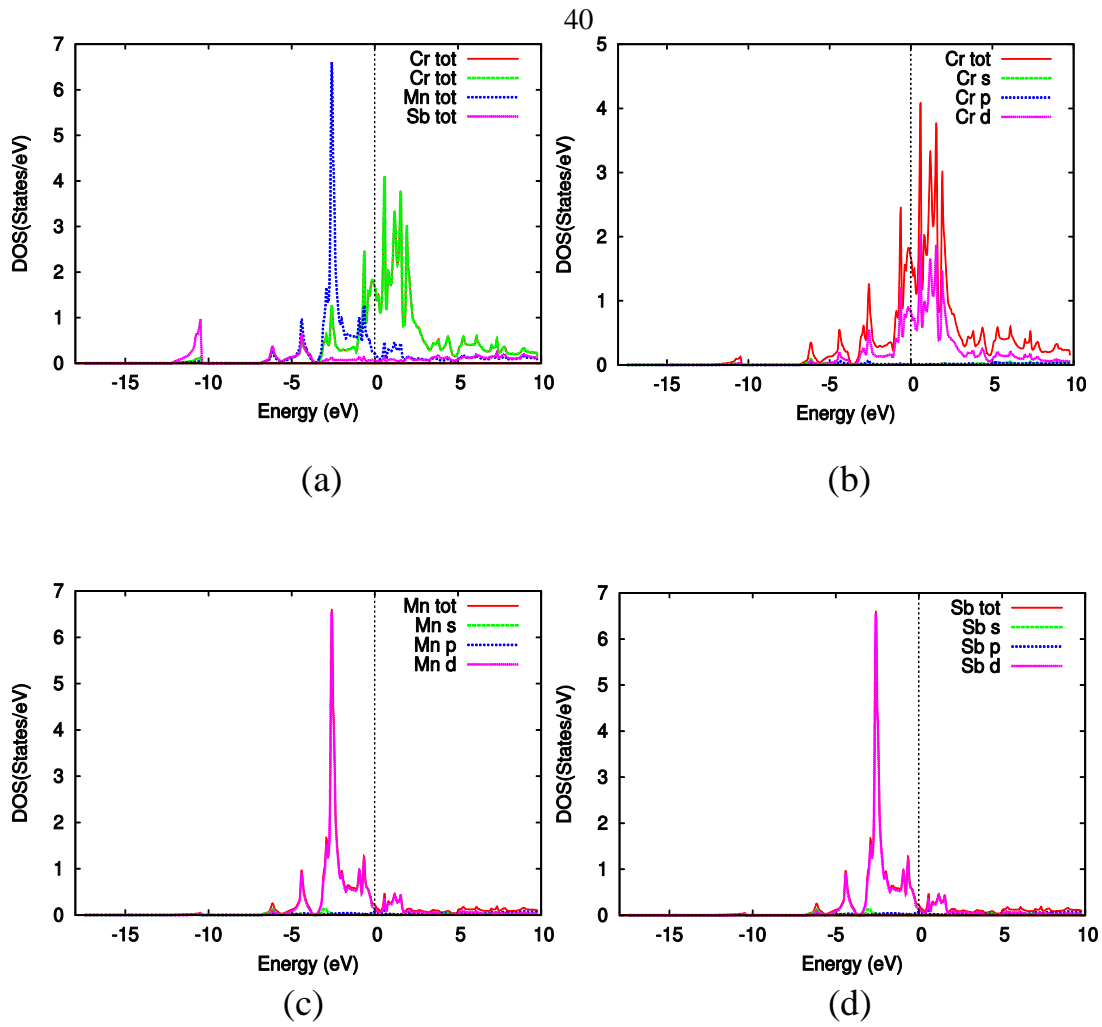


Figure 22: (a) Total density of states of spin up for normal Cr_2MnSb and partial density of states of spin up for (b) Cr atom (c) Mn atom (d) Sb atom of normal Cr_2MnSb compound.

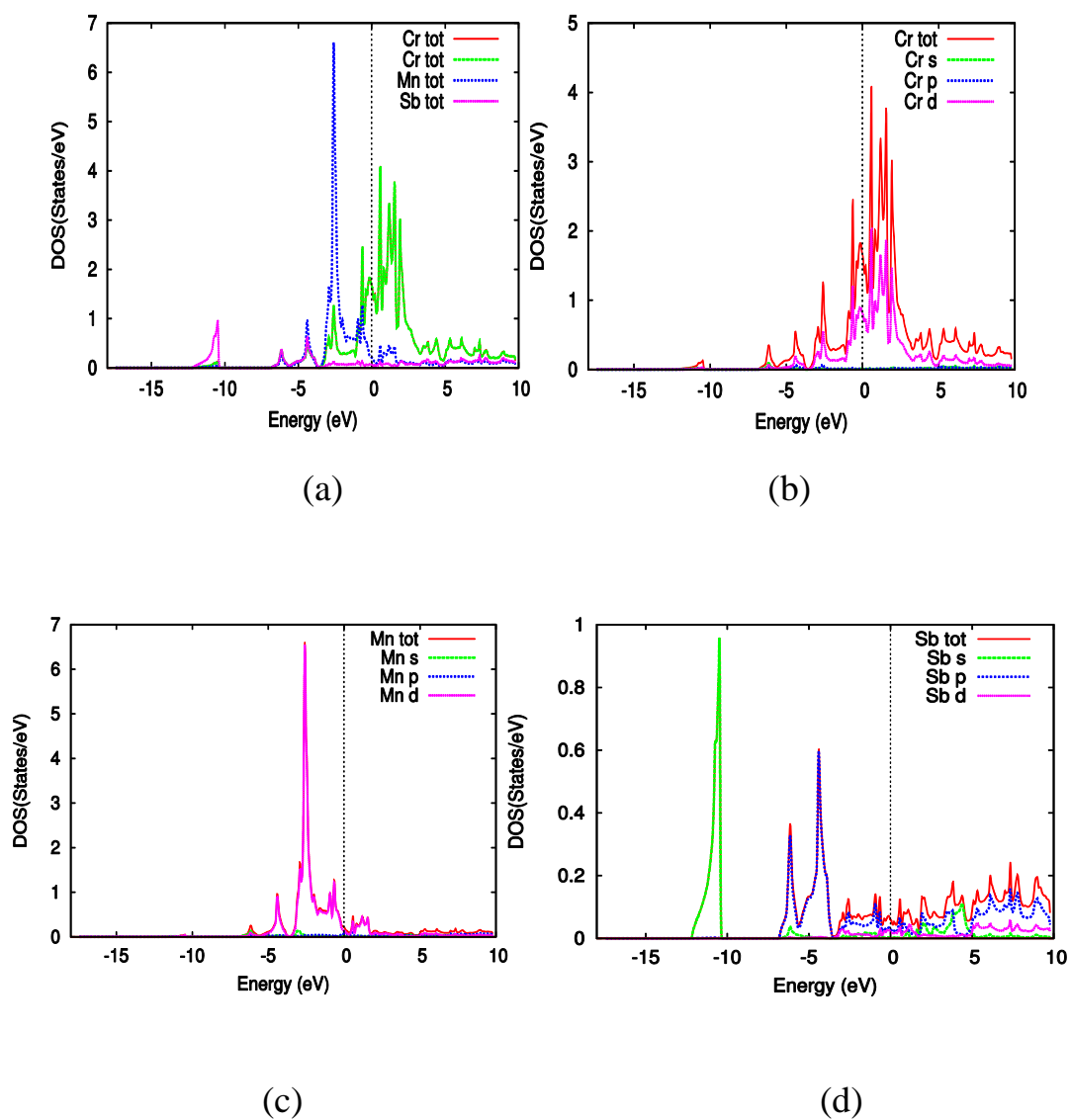


Figure 23: (a) Total density of states of spin down for normal Cr_2MnSb and partial density of states of spin up for (b) Cr atom (c) Mn atom (d) Sb atom of normal Cr_2MnSb compound.

3.5. Elastic properties

In this section, we have calculated bulk modulus (B), shear modulus (S), elastic constants (C_B), B/S ratio, Poisson's ratio, Young's modulus (Y) and anisotropic factor (A) of the normal and inverse Heusler (Co_2CrAl , Cr_2MnSb) compounds. For cubic crystal, the standard mechanical stability is $C_{11} > 0$, $C_{11} + C_{12} > 0$, $C_{11} - C_{12} > 0$ and $C_{44} > 0$ ^[33].

Our calculations for normal and inverse Heusler (Co_2CrAl , Cr_2MnSb) compounds are presented in Table 8. We found that the normal and inverse Heusler Co_2CrAl are mechanically stable. Whereas, the inverse Cr_2MnSb is mechanically instable in ferromagnetic state. On the other hand the normal Cr_2MnSb is mechanically stable in the ferromagnetic state.

We have used Voigt approximation^[34] to calculate the shear modulus and bulk modulus. Voigt shear modulus S_v can be calculated from the following equation:

$$S_v = \frac{1}{5}(C_{11} - C_{12} + 3C_{44}) \quad (22)$$

Bulk modulus for cubic structure is given by the following:

$$B = \frac{1}{3}(C_{11} + 2C_{12}) \quad (23)$$

The definition for the ratio of the stress to strain is the Young modulus (Y) is given by the following:

$$Y = \frac{9BS_v}{(S_v + 3B)} \quad (24)$$

Anisotropic factor and Poisson's ratio is given by the following:

$$A = \frac{2C_{44}}{C_{11}-C_{12}} \quad (25)$$

$$\nu = \frac{3B-2S_\nu}{2(3B+S_\nu)} \quad (26)$$

The Bulk modulus and shear modulus measure the hardness of materials^[35]. Therefore the ratio B/S measures the brittleness and ductility of the materials, when B/S>1.75 the material behaves in ductile nature. Otherwise it behaves in a brittle nature^[36]. From present calculations in Table 8, the B/S ratio of inverse and normal Heusler Co_2CrAl compound are 3.7019 and 2.0658, respectively. Depending on the B/S ratio values both inverse and normal have ductile natures. The B/S ratio values for inverse and normal Heusler Cr_2MnSb compound are found to be 1.572 and 4.36280, respectively. Depending on the B/S ratio values the inverse Heusler Cr_2MnSb compound has brittle nature and the normal Heusler Cr_2MnSb compound has ductile nature.

Young modulus (Y) measures the stiffness of materials. The highest the value of Young modulus (Y), the stiffer the material is. The stability of material and the nature of bonding have measured by the Poisson's ratio. When Poisson's ratio is greater than 1/3, the material behaves in ductile nature otherwise it behaves as brittle nature^[37]. From present calculations in Table 8, the Poisson's ratio of inverse and normal Heusler Co_2CrAl compound are 0.376 and 0.291, respectively. Depending on the Poisson's ratio values both inverse and normal have ductile natures. The Poisson's ratio values for inverse and normal Heusler Cr_2MnSb compound are

found to be 0.393 and 0.903, respectively. Depending on the Poisson's ratio values the inverse Heusler Cr_2MnSb compound has brittle nature and the normal Heusler Cr_2MnSb compound has ductile nature. Poisson's ratio for covalent bonds compounds is too lower than 0.25 for pure covalent bonds, while for ionic bonds compounds from 0.25 to 0.5. From Table 8, the normal and inverse Heusler (Co_2CrAl , Cr_2MnSb) compounds have ionic bonds. Likewise, the elastic anisotropy is an important parameter to measure the degree of anisotropy of materials ^[38]. For an isotropic material, the value of A is unity. Otherwise the material has an elastic anisotropy ^[39]. From the present values of the anisotropy (Table 8) for inverse and normal Heusler Co_2CrAl compound are found to be 6.697 and 3.114, respectively. The anisotropy for normal Heusler Cr_2MnSb compound is found to be 4.732. The normal and inverse Heusler (Co_2CrAl , Cr_2MnSb) compounds are anisotropy elastic.

Table 8: Voigt bulk modulus (B), Voigt shear modulus (S), elastic constants (C_B), B/S ratio, Voigt Poisson's ratio (ν), Voigt Young's modulus (Y) and anisotropic factor (A) of the FM normal and inverse Heusler (Co_2CrAl , Cr_2MnSb) compounds.

Materials	C_{11} (GPa)	C_{12} (GPa)	C_{44} (GPa)	B (GPa)	S (GPa)	B/S	Y (GPa)	ν	A
Normal Co_2CrAl	268.592	169.462	154.343	202.505	98.029	2.0658	253.226	0.291	3.114
Inverse Co_2CrAl	275.6864	234.2043	138.9022	248.03	67	3.7019	184.396	0.376	6.697
Inverse Cr_2MnSb	197.1538	138.7903	-488.5573	158.244	-100.664	1.57200	-383.259	0.903	-16.7
Normal Cr_2MnSb	267.3836	224.7424	100.9041	238.955	54.771	4.36280	152.65	0.393	4.732

Chapter Four

Conclusion

In this work, we have studied the structural, magnetic, electronic and elastic properties of inverse and normal Heusler (Co_2CrAl , Cr_2MnSb) compounds. We found that the normal Heusler (Co_2CrAl), normal, inverse Heusler (Cr_2MnSb) and tetragonal (139) Heusler (Co_2CrAl , Cr_2MnSb) compounds are half-metals, thus half-metallic nature is a promising material for future spintronic applications. The normal Heusler Co_2CrAl compound has an indirect energy band gap of 0.6 eV within PBE-GGA method. The energy band gap within mBJ-GGA for normal Heusler Co_2CrAl compound is found to be 0.9 eV. The inverse and normal Heusler (Cr_2MnSb) compounds have direct energy band gap of 0.8 eV and 0.9 eV, respectively within PBE-GGA method. The energy band gap within mBJ-GGA for inverse and normal Heusler (Cr_2MnSb) compounds are found to be 0.9 eV and 1 eV, respectively. The tetragonal Heusler (Co_2CrAl , Cr_2MnSb) compounds have direct energy band gap and found to be 0.8 eV and 0.9 eV, respectively within PBE-GGA method. We have found that the normal Heusler Co_2CrAl is a ferromagnetic compound with total magnetic moment of $M^{tot} = 3 \mu_B$. On the other hand, the total magnetic moment for inverse Co_2CrAl compound is $M^{tot} = 0.83116 \mu_B$. The normal and tetragonal Heusler (Cr_2MnSb) compounds have a small total magnetic moment which means that this compound is ferrimagnetic. We found from elastic constants calculations that normal and inverse Heusler Co_2CrAl are mechanically stable, but inverse Cr_2MnSb is mechanically instable in

ferromagnetic state. On the other hand, the normal Cr_2MnSb is mechanically stable in the ferromagnetic state. B/S results show that normal Heusler (Cr_2MnSb) compound, normal and inverse Heusler Co_2CrAl have ductile natures, but the inverse Heusler Co_2CrAl has brittle nature. On the other hand, from the Poisson's ratio values we found that the normal and inverse Heusler (Co_2CrAl , Cr_2MnSb) compounds have ionic bonds. Finally, the normal and inverse Heusler (Co_2CrAl , Cr_2MnSb) compounds are anisotropy elastic.

References

1. de Groot R. A., Müller F. M., van Engen P. G. and Buschow K. H., 1983. **New Class of Materials: Half-Metallic Ferromagnets** *Phys. Rev. Lett.*, 50:2024.
2. Blum C. F., Ouardi S., Fecher G. H., Balke B. Kozina X., Stryganyuk G., Ueda S., Kobayashi K., Felser C. and Wurmehl B., 2011. **Electronic Structure and Physical Properties of Heusler Compounds for Thermoelectric and Spintronic Applications** *Phys. Lett.*, 98:252501.
3. Ouardi S., Fecher G., Balke B., Kozina X., Stryganyuk G., Felser C., Lowitzer S., Mödderitzsch D., Ebert H. and Ikenaga E., 2010. **Structural and magnetic characterization of Fe_2CrSi Heusler alloy nanoparticles as spin injectors and spin based sensors**, *Phys. Rev. B*, 82:085108.
4. Heusler F., 1903. **"Über magnetische Manganlegierungen"**. *Verhandlungen der Deutschen Physikalischen Gesellschaft (in German)*.
5. Aquil Ahmad, A. K. Das, and S. K. Srivastava, **Competition of L21 and XA Ordering in Fe_2CoAl Heusler Alloy: A First-Principles Study**, *Department of Physics, Indian Institute of Technology Kharagpur, India-721302*.
6. Dowben P., 2007. **Half Metallic Ferromagnets**, *Condens. Matter*, 19 310301.

7. Dai X.F., Liu G.D., Chen L.J., Xiao G. and Wu G.H., 2006. ***Mn₂CoSb* compound: structural, electronic, transport and magnetic properties**, Solid State Commun. 140 533.
8. Liu G.D., Dai X.F., Liu H.Y., Chen J.L., Li Y.X., 2008. ***Mn₂CoZ* (Z=Al, Ga, In, Si, Ge, Sn, Sb) compounds: structural, electronic, and magnetic properties**, Phys. Rev. B 77, 014424.
9. Bayar E., Kervan N.v and Kervan S., 2011 . **Half-metallic ferrimagnetism in the *Ti₂CoAl* Heusler compound**, J. Magn. Magn. Mater. 323 2945.
10. Fang Q.L., Zhang J.M., Xu K.W. and Ji V., 2013. **Electronic structure and magnetism of *Ti₂FeSi*: a first-principles study**, J. Magn. Magn. Mater. 345 171.
11. Kervan N., S., 2012. **A first-principle study of half-metallic ferrimagnetism in the *Ti₂CoGa* Heusler compound**, J. Magn. Magn. Mater. 324 645.
12. Jia H.Y., Dai X.F., Wang L.Y., Liu R., Wang X.T., Li P.P., Cui Y.T. and Liu G.D., 2014. **Doping effect on electronic structures and band gap of inverse Heusler compound: *Ti₂CrSn***, J. Magn. Magn. Mater. 367 33.
13. Birsan A., Palade P. and Kuncser V., 2013. **Prediction of half metallic properties in *Ti₂CoSi* Heusler alloy based on density functional theory**, J. Magn. Magn. Mater. 331 109.
14. Yamamoto M., Marukame T., Ishikawa T., Matsuda K., Uemura T. and Arita M., 2006. **Fabrication of fully epitaxial magnetic tunnel**

- junctions using cobalt-based full- Heusler alloy thin film and their tunnel magnetoresistance characteristics**, J. Phys. D Appl. Phys. 39 , 824.
15. S. Kammerer, A. Thomas, A. Hütten, G. Reiss, ***Co₂MnSi* Heusler alloy as magnetic electrodes in magnetic tunnel junctions**, Appl. Phys. Lett. 85 (2004) 79.
 16. Okamura S., Miyazaki A., Sugimoto S., Tezuka N. and Inomata K., 2005. **Large tunnel magnetoresistance at room temperature with a *Co₂FeAl* full-Heusler alloy electrode**, Appl. Phys. Lett. 86, 232503.
 17. Sakuraba Y., Hattori M., Oogane M., Ando Y., Kato H., Sakuma A., Miyazaki T. and Kubota H., 2006. **Electronic structure, magnetism and disorder in the Heusler compound *Co₂TiSn***, Appl. Phys. Lett. 88, 192508.
 18. Sakuraba Y., Miyakoshi T., Oogane M., Ando Y., Sakuma A., T., Kubota H., 2006. **Electronic structure, magnetism, and disorder in the Heusler compound *Co₂TiSn***, Appl. Phys. Lett. 89, 0528508.
 19. Zhang M., Liu Z., Hu H., et al. , 2004. **Is Heusler compound *Co₂CrAl* a half-metallic ferromagnetic band structure, and transport properties** Magnetism and Magnetic Materials, 277 ,130–135.
 20. Hakimi M., Kameli P. and Salamati H., 2010. **Structural and magnetic properties of *Co₂CrAl* Heusler alloys prepared by mechanical alloying**, Magnetism and Magnetic Materials.

21. Ozdogan K. and Galanakis I., 2009. **First-principles electronic and magnetic properties of the half-metallic antiferromagnet Cr_2MnSb** *Magnetism and Magnetic Materials*, 321 , L34–L36.
22. Gupta S., Matsukura F. and Ohno H., 2019. **Properties of sputtered full Heusler alloy Cr_2MnSb and its application in a magnetic tunnel junction**, *Applied Physics*.
23. Hirohata A., Huminiuc T., Sinclair J., Wu H., Samiepour M., Fernandez G., O'Grady K., Balluf J., Meinert M. and Reiss G., **Development of antiferromagnetic Heusler alloys for the replacement of iridium as a critically raw material**, *Applied Physics*, (Vol. 50, Issue 44).
24. Abu Baker D., Abu-Jafar M., Mousa A., Jaradat R., Ilaiwi K. and Khenata R., 2020. **Structural, magnetic, electronic and elastic properties of half-metallic ferromagnetism full-Heusler alloys: Normal- Co_2TiSn and inverse- Zr_2RhGa using FP-LAPW method**, *Materials Chemistry and Physics*.
25. Blaha P., Schwarz K., Georg K., Madsen H., Kvasnicka D., Luitz J., Laskowski R., Tran F. and Laurence D., 2019. **An Augmented PlaneWave Plus Local Orbitals Program for Calculating Crystal Properties**, User's Guide, WIEN2k 19.1.
26. Schwarz K., 2003. **DFT calculations of solids with LAPW and WIEN2k**, Institute of Materials Chemistry, Vienna University of Technology.

27. Camargo-Martinez J. A. and Baquero R. 2012, **Performance of the modified Becke-Johnson potential**, Materials Science.
28. Blaha P., Schwarz K., Madsen G., Kvasnika D. and Luitz J., 2001. **WIEN2k**, Technical Universitat Wien, Austria.
29. Blaha P., Schwarz K., Madsen G., Kvasnika D. and Luitz J., 2001. **WIEN2k**, Technical Universitat Wien, Austria, ISBN 3-9501031-1-2.
30. Monkhorst H. J. and Pack I.D., 1976. **Phys. Rev. B** 13 5188.
31. Murnaghan F. D., 1944. "**The Compressibility of Media under Extreme Pressures**", National Academy of Sciences of the United States of America.
32. Kandpal H., Ksenofontov V., Wojcik M., Seshadri R. and Claudi Felser, *Electronic structure, magnetism and disorder in the Heusler compound Co_2TiSn* , **Journal of Physics**.
33. Galanakis I., 2002. **Surface properties of the half- and full-Heusler alloys**, CONDENSED MATTER.
34. Hung Z. W., Zhao Y. H., Hou H., and Han P. D., 2012. **Physica B** 407 1075 .
35. Voigt W., Kristallphysik L. and Teubner B.G., 1850. Berlin, Germany, 1910, p.
36. Teter D. M., (1998). **Computational alchemy: the search for new superhard materials**, MRS Bull. 23 , 22.
37. Pugh S. F., (1954) .**The London, edinburgh and dublin philosophical magazine and, J. Sci.** 45 , 823.

38. Zener C., 1948. **lasticity and Anelasticity of Metals**, University of Chicago Press, Chicago.
39. Ravindran P., Fast L., Korzhavyi P.A.and Johansson B., (1998). **Density functional theory for calculation of elastic properties of orthorhombic crystals: application to TiSi₂**, J. Appl. Phys. 84 ,4891.

جامعة النجاح الوطنية

كلية الدراسات العليا

الخصائص التركيبية والالكترونية والمغناطيسية والمرونية
لمركبات هزلة الطبعفة والمعكوسة : Co_2CrAl , Cr_2MnSb
بأستخدام الجهد التام

أعداد

سارة جمال محمد يحف

أشراف

أ. د. محمد أبو جعفر

قدمت هذه الأطروحة أستكمالاً لمتطلبات الحصول على درجة الماجستير في الففزيااء في كلية الدراسات العليا في جامعة النجاح الوطنية، نابلس- فلسطين.

2021

ب

الخصائص التركيبية والالكترونية والمغناطيسية والمرونية
لمركبات هزلر الطبيعية والمعكوسة: Co_2CrAl , Cr_2MnSb

باستخدام الجهد التام

اعداد

سارة جمال محمد يحيى

اشراف

أ. د. محمد أبو جعفر

الملخص

تم فحص الخصائص التركيبية والالكترونية والمغناطيسية والمرونية لمركبات هزلر الطبيعية والمعكوسة (Co_2CrAl , Cr_2MnSb) عن طريق استخدام الجهد النظرية الكثافة الوظيفية (DFT) والجهد التام المزيد ذو الموجات المستوية الخطية (FP-LAPW) والتقريب التدريجي المعمم (PBE-GGA) ضمن اطار برنامج WIEN2k.

تم استخدام التقريب التدريجي المعمم (GGA) لحساب ثابت الشبكة (a) ومعامل الصلابة (B) ومشتقة معامل الصلابة بالنسبة للضغط (B') وأيضا تم استخدام نظام بيكي جونسون لتحسين فجوة الطاقة.

من أهم نتائج هذه الدراسة:

1. تبين أن المركبات Co_2CrAl الطبيعي، Cr_2MnSb العكسي و Cr_2MnSb الطبيعي تمتلك الخاصية النصف معدنية.
2. تبين أن المركب Co_2CrAl العكسي يمتلك الخاصية المعدنية.
3. تبين أن المركبين Co_2CrAl العكسي و Co_2CrAl الطبيعي يمتلكان خواص مغناطيسية.
4. تبين ان النتائج التي اوجدناها قريبة من النتائج العملية والنظرية الاخرى.
5. من خلال الخواص المرونية تبين أن المركبين Co_2CrAl العكسي و Co_2CrAl الطبيعي مستقران ميكانيكيا.
6. تبين أن المركب Cr_2MnSb العكسي قابل للطرق والسحب.

ج

7. تبين أن المركبات Cr_2MnSb الطبيعي، Co_2CrAl العكسي و Co_2CrA الطبيعي هشات
للانكسار.

